Molecular Therapy
Original Article

AAV-mediated gene therapy for focal epilepsy by expressing neuropeptide Y and Y2 receptor in rodent and non-human primate hippocampus

Barbara Terzic,[1,8] Esbjörn Melin,[2,8] Pernilla Fagergren,[2] David Dobry,[1] Stefano Cattaneo,[3] Iris Giupponi,[4] Barbara Bettegazzi,[4,5] Michele Simonato,[4,6] Karin Agerman,[2] Merab Kokaia,[2,7] Lawrence Moon,[1] and Elizabeth Ramsburg[1]

[1]Spark Therapeutics, Inc., Philadelphia, PA 19104, USA; [2]CombiGene AB, 114 34 Stockholm, Sweden; [3]IRCCS Neuromed, 86077 Pozzilli IS, Italy; [4]Division of Neuroscience, IRCCS San Raffaele Scientific Institute, 20132 Milan, Italy; [5]Vita-Salute San Raffaele University, 20132 Milan, Italy; [6]Department of Neuroscience and Rehabilitation, University of Ferrara, 44121 Ferrara, Italy; [7]Epilepsy Center, Department of Clinical Sciences, Lund University, 221 00 Lund, Sweden

Epilepsy affects approximately 50 million people worldwide, and over 30% of patients are considered treatment resistant to currently available anti-seizure drugs. Neuropeptide Y (NPY) has been shown to inhibit excitatory synaptic transmission in hippocampal slices from human epilepsy patients via Y2 receptors (Y2Rs), and overexpression of NPY and/or Y2R in the hippocampus reduces seizures in rodent models of epilepsy. In this study, we demonstrate that AAV-mediated delivery of NPY and Y2R using a novel vector (SPK100.NPY-Y2R) inhibits seizures in rodents. SPK100.NPY-Y2R reduced spontaneous neuronal activity in primary rat cortical cultures and attenuated evoked neuronal activity in *ex vivo* slices of mouse hippocampus. Furthermore, intrahippocampal administration of SPK100.NPY-Y2R reduced the progression and duration of seizures in a rat model of rapid kindling. Parallel experiments confirmed that hippocampal overexpression of NPY and Y2R is also sufficient to reduce spontaneous seizures in a genetic mouse model of epilepsy (synapsin triple knockout). We also demonstrated successful magnetic resonance-guided convection enhanced delivery of SPK100.NPY-Y2R to the hippocampus of *Papio hamadryas* (baboon). This approach achieved favorable vector biodistribution and transduction in the hippocampus, with no observed adverse events. These findings support the development of an intrahippocampal AAV.NPY-Y2R therapy for treating seizures in patients with temporal lobe epilepsy.

INTRODUCTION

Epilepsy is a chronic neurological disorder, characterized by spontaneous and recurrent seizures, that affects around 50 million people worldwide.[1] Temporal lobe epilepsy (TLE) comprises a major part of focal epilepsy cases, wherein seizures can originate from the structures of the temporal lobe such as the hippocampus and surrounding areas.[2,3] In addition to seizures, patients can experience cognitive impairment, mood changes, and hippocampal sclerosis and degeneration, significantly impacting quality of life and increasing risk for early mortality.[4–7] Unfortunately, upward of 30% of all epilepsy patients are refractory to currently available anti-seizure medications, highlighting the urgent need to develop additional therapies for the management and treatment of seizures in this patient population.[8]

Neuropeptide Y (NPY) has been reported to exhibit anti-seizure effects, primarily in the hippocampus but also in other brain regions.[9–13] NPY is typically upregulated in the hippocampus after seizure induction; NPY knockout mice present with increased susceptibility to both electrical kindling and chemoconvulsant-induced seizures; and intracerebroventricular delivery of recombinant NPY abrogates EEG-detected seizures in the hippocampus of mice.[14–17] Bath application of NPY is also capable of reducing evoked excitatory transmission at Schaffer collateral-CA1 synapses of the hippocampus in resected epileptic tissue from human TLE patients.[13,18] NPY is a 36-amino-acid neuropeptide primarily released from pre-synaptic terminals of GABAergic neurons through dense core vesicles in response to high-frequency burst firing. It serves as an endogenous modulator of synaptic transmission via the NPY receptor family of G-protein-coupled receptors (GPCRs) including Y1, Y2, Y4, and Y5.[19–21] The NPY Y2 receptor (Y2R) is a pre-synaptically localized GPCR highly expressed in the hippocampus, where it functions to reduce neurotransmitter release by decreasing intracellular cAMP levels and inhibiting voltage-gated Ca^{2+} channel activity.[22,23] Previous studies have supported a role for Y2R in mediating the seizure-suppressant effects of NPY through pre-synaptic inhibition of glutamate release, and have shown Y2R upregulation following seizures in rodent models and human patients with TLE.[13,18,24–28] Therefore, the endogenous NPY-Y2R signaling pathway can be

Received 4 December 2024; accepted 11 June 2025;
https://doi.org/10.1016/j.ymthe.2025.06.019.

[8]These authors contributed equally

Correspondence: Esbjörn Melin, CombiGene AB, 114 34 Stockholm, Sweden.
E-mail: esbjornmelin@hotmail.com

leveraged to mitigate the aberrant excitatory neurotransmission occurring during seizures.

Localized delivery of a gene therapy in focal epilepsy patients could serve as an alternative to surgical resection or focal ablation for those who are drug-refractory and have limited treatment options, or could provide a treatment option for the sub-population of patients not eligible for surgery.[29–31] Recombinant adeno-associated viral (rAAV) vectors provide several advantages for targeted delivery of genetic therapies *in vivo*, including their relative safety and low immunogenicity compared with other viral modalities, as well as their ability to transduce a variety of cell types, including non-dividing cells such as neurons of the brain.[32–34] Furthermore, AAV-mediated overexpression of NPY and/or Y2R has been shown to reduce seizures in rodent models of epilepsy, with co-administration of rAAV-NPY and rAAV-Y2R into the rat hippocampus conferring an additive, anti-seizure effect in an electrical kindling model of seizures.[35–37] In contrast, NPY action at Y1 receptors has been reported to facilitate seizure activity.[38–40] Therefore, our dual NPY-Y2R approach aims to boost Y2R-mediated signaling of NPY to confer seizure suppression.

In this study, we build on these previous findings by utilizing our bioengineered capsid, AAV-Spark100, to deliver human NPY and human Y2R (referred to as SPK100.NPY-Y2R) to the hippocampus of both rodents and non-human primates. AAV-Spark100 is a bioengineered capsid originally described in a clinical trial for a hemophilia B gene therapy with demonstrated safety in human patients.[41] Our findings demonstrate the anti-seizure effects of AAV-Spark100-mediated NPY and Y2R overexpression across relevant *in vitro*, *ex vivo*, and *in vivo* rodent models. We also report the first successful AAV delivery to the *Papio hamadryas* (baboon) NHP's hippocampus, demonstrating precise hippocampal vector biodistribution with minimal off-target spread beyond the targeted structure. These findings lend further support toward the development of this therapy for treating seizures in patients with TLE.

RESULTS

SPK100.NPY-Y2R reduces spontaneous neural activity *in vitro*

SPK100.NPY-Y2R is a single-stranded, rAAV vector consisting of a bioengineered capsid (AAV-Spark100) and an expression cassette containing the human NPY coding sequence and human Y2R coding sequence separated by an internal ribosomal entry site (IRES) and downstream of a ubiquitously active, cytomegalovirus immediate-early enhancer/β-actin (CAG) promoter (hereafter referred to as SPK100.NPY-Y2R). The vector also contains a modified woodchuck hepatitis virus post-transcriptional regulatory element (WPRE) and the bovine growth hormone polyadenylation sequence (BGHpA), as previously described.[26] See further details on vector design and production in materials and methods.

Intracellular calcium ion (Ca^{2+}) concentrations can be visualized *in vitro* and *in vivo* using fluorescent Ca^{2+} indicators providing a measure of cell activity.[42,43] To assess the effects of NPY and Y2R overexpression on neuronal activity, we applied an *in vitro* system for long-term monitoring of spontaneous activity of rat primary cortical neurons via Ca^{2+} imaging (Figure 1A). First, experiments with an AAV-Spark100 reporter vector (SPK100.CAG-eGFP) confirmed the ability of AAV-Spark100 to transduce approximately 95% of rat primary cortical neurons *in vitro* (indicated by GFP expression and immunopositivity for microtubule-associated protein 2 [MAP2; a neuron-specific cytoskeletal protein]) at 5×10^6 vector genomes (vg) per cell with a small reduction in cell viability (Figures S1A and S1B). As expected, spontaneous activity of rat cortical neurons significantly increased over time in culture under control conditions (Figures 1B–1E). Over 35 days in culture, both the total number of active neurons and the average neuronal activity were significantly reduced in SPK100.NPY-Y2R-treated wells compared with mock-treated (vehicle) wells (Figures 1B and 1C). The average neuronal burst rate and burst strength were also significantly reduced in SPK100.NPY-Y2R-treated wells versus mock-treated wells (Figures 1D and 1E). In a parallel experiment, AAV9-mediated delivery of NPY and Y2R similarly attenuated neuronal activity when compared with a negative control AAV (Figures S1C–S1F). These results collectively demonstrate a significant reduction in primary rat cortical neuron activity upon AAV-mediated delivery of NPY and Y2R.

NPY peptide or SPK100.NPY-Y2R attenuate evoked circuit activity in slices of mouse hippocampus *ex vivo*

We next used microelectrode array (MEA) recordings to capture population activity of intact, neuronal networks, providing spatial resolution within the hippocampal microcircuit.[44,45] Transverse, *ex vivo* hippocampal slices were harvested from adult, male mice, and both spontaneous and 4-aminopyridine(4-AP)-evoked network activity was measured using an MEA system (see materials and methods for details). Bath application of NPY peptide did not affect spontaneous activity measured from the hippocampal CA1 subfield of *ex vivo* slices at any dose prior to 4-AP addition (Figures S2A and S2B). However, bath application of NPY peptide dose dependently and significantly reduced the number of 4-AP-evoked spikes and bursts measured from the hippocampal CA1 subfield compared with baseline, with the most pronounced effect observed at 1 μM (Figures 2A and 2B; $n = 8$ slices per group, 1–3 slices per mouse from 3 to 5 mice). Concomitant application of a Y2R inhibitor (BIIE0246; 0.6 μM) trended toward attenuating the effects of NPY peptide at 1 μM on 4-AP evoked spiking (unpaired t test, $p = 0.05$) and bursting (unpaired t test, $p = 0.09$) activity in the hippocampal CA1, suggesting that the inhibitory effects of NPY are at least partially mediated by Y2R at this dose (Figures 2A and 2B).[46] Similar results of NPY and Y2R inhibitor application were obtained in the hippocampal CA3 subfield (data not shown). To validate the utility of the MEA approach in detecting inhibitory effects on evoked neuronal activity, a high dose of Retigabine, a voltage-gated potassium channel opener, was bath applied to the slices, demonstrating suppression of 4-AP evoked activity at 10 μM (a clinically supra-physiological [higher than expected at the therapeutic dose range] concentration).[47,48] These results confirm that bath application of NPY reduces network excitability evoked by 4-AP, likely by

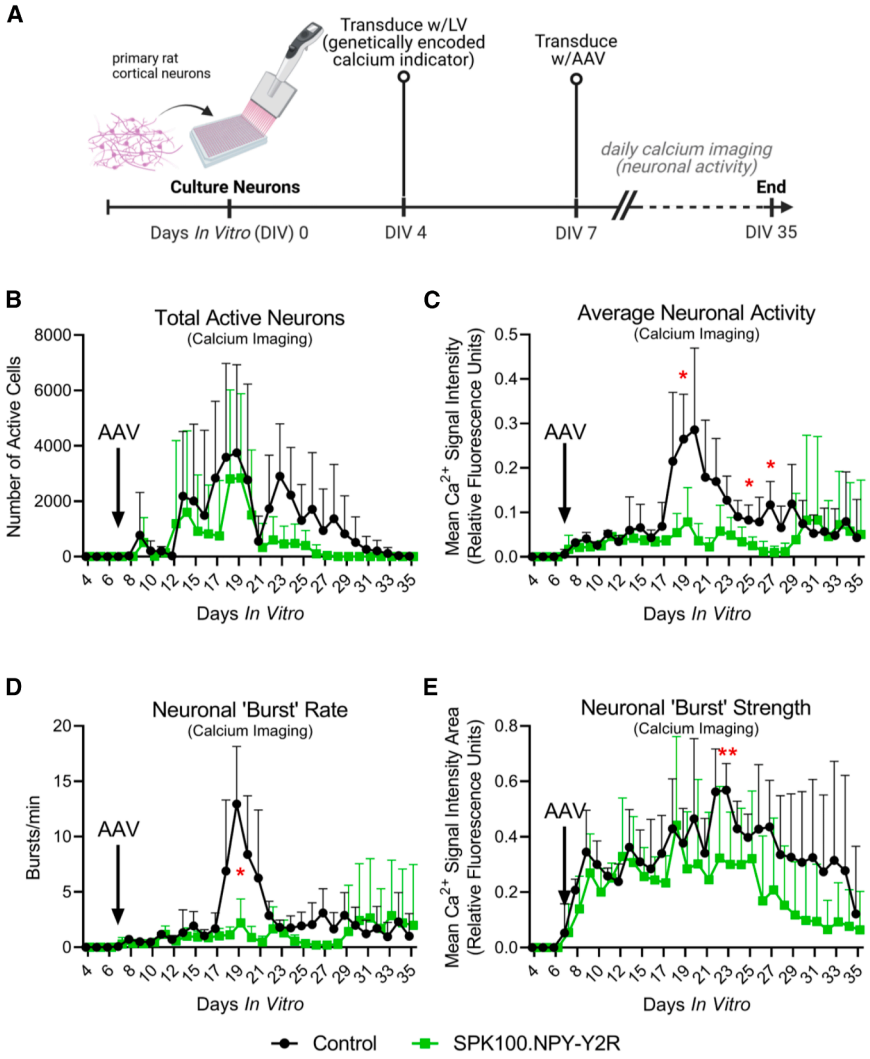

Figure 1. Spontaneous neural activity is attenuated by SPK100.NPY-Y2R in primary rat cortical cultures

(A) Schematic describing experimental timeline. Primary rat cortical neurons were cultured *in vitro* (day *in vitro* [DIV0]). On DIV4, cells were transduced with a lentivirus delivering a genetically encoded calcium indicator (Incucyte Neuroburst Orange Lentivirus, Sartorius, cat. no. 4736), and received either SPK100.NPY-Y2R (5×10^6 vg per cell; green line) or mock treatment (black line) on DIV7. Calcium ion (Ca^{2+}) signal was measured and recorded daily until DIV35. (B) The number of active neurons (number of objects that burst at least once above the minimum burst threshold over the total scan time) was significantly reduced in SPK100.NPY-Y2R-treated cells compared to mock-treated control cells (effect of time, $p < 0.0001$; effect of treatment, $p = 0.0038$; effect of interaction, ns). (C) The mean Ca^{2+} signal intensity (mean fluorescence intensity of an object over the total scan time, averaged across all objects) was significantly reduced over time in SPK100.NPY-Y2R-treated neurons versus mock-treated control neurons (effect of time, $p < 0.001$; effect of treatment, $p < 0.0001$; effect of interaction, $p < 0.0001$). (D) The mean burst rate (the number of Ca^{2+} bursts over the total scan time divided by the scan time) was significantly reduced over time in SPK100.NPY-Y2R-treated neurons versus mock-treated control neurons (effect of time, $p < 0.0001$; effect of treatment, $p = 0.0012$; effect of interaction, $p < 0.0001$). (E) The mean burst strength (the area under each Ca^{2+} burst divided by the duration of that burst, averaged across all bursts) was significantly decreased in SPK100.NPY-Y2R-treated neurons versus mock-treated control neurons (effect of time, $p < 0.0001$; effect of treatment, $p = 0.0022$; effect of interaction, ns). All data: mixed effects analysis followed by a Šídák's multiple comparisons test (*$p < 0.05$, **$p < 0.01$). Data are represented as mean +standard deviation. n = 8–16 wells per condition per time point. LV, lentivirus; AAV, adeno-associated virus.

decreasing excitatory transmission in the mouse hippocampus in a Y2R-dependent manner.

To evaluate the effects of AAV-mediated NPY and Y2R overexpression, a separate experiment was conducted in which mice received bilateral, intrahippocampal delivery of either vehicle (vector diluent) or SPK100.NPY-Y2R at varying doses (3×10^9, 9.5×10^9, or 3×10^{10} vg per hippocampus; 6×10^9, 1.9×10^{10}, or 6×10^{10} vg total per animal) 3 weeks before harvesting hippocampal slices for *ex vivo* MEA recordings. SPK100.NPY-Y2R pre-treatment dose dependently and significantly reduced the number of 4-AP-evoked spikes and showed a trend to reducing the number of bursts in the hippocampal CA1 subfield when compared with diluent-injected controls (Figures 2C and 2D; n = 10 slices per group; 1 slice per mouse from 10 mice). Similar effects were seen in the hippocampal CA3 subfield (Figures S2C and S2D). Importantly, circuit activity recorded at baseline (before 4-AP) was not significantly different in SPK100.NPY-Y2R-treated hippocampi (CA1) versus diluent-treated controls (Figures S2E and S2F). Analysis of all slices used for MEA recordings confirmed a dose-dependent and significant increase in vector genome copies and NPY protein abundance in the hippocampus of SPK100.NPY-Y2R-treated mice compared with diluent-injected controls (Figures 2E and 2F). NPY protein abundance was also significantly and positively correlated with vector genome copies detected in each hippocampal slice (Figure S2G). Furthermore, the number of 4-AP-evoked spikes measured from the hippocampal CA1 was significantly reduced with increasing NPY protein abundance (Figure 2G). These results build on the data using NPY bath application and confirm that AAV-mediated overexpression of NPY and Y2R can significantly attenuate evoked excitatory transmission in the hippocampal microcircuit of mice.

Given that NPY is also a well-established orexigenic factor that influences feeding behavior and body weight through its actions on

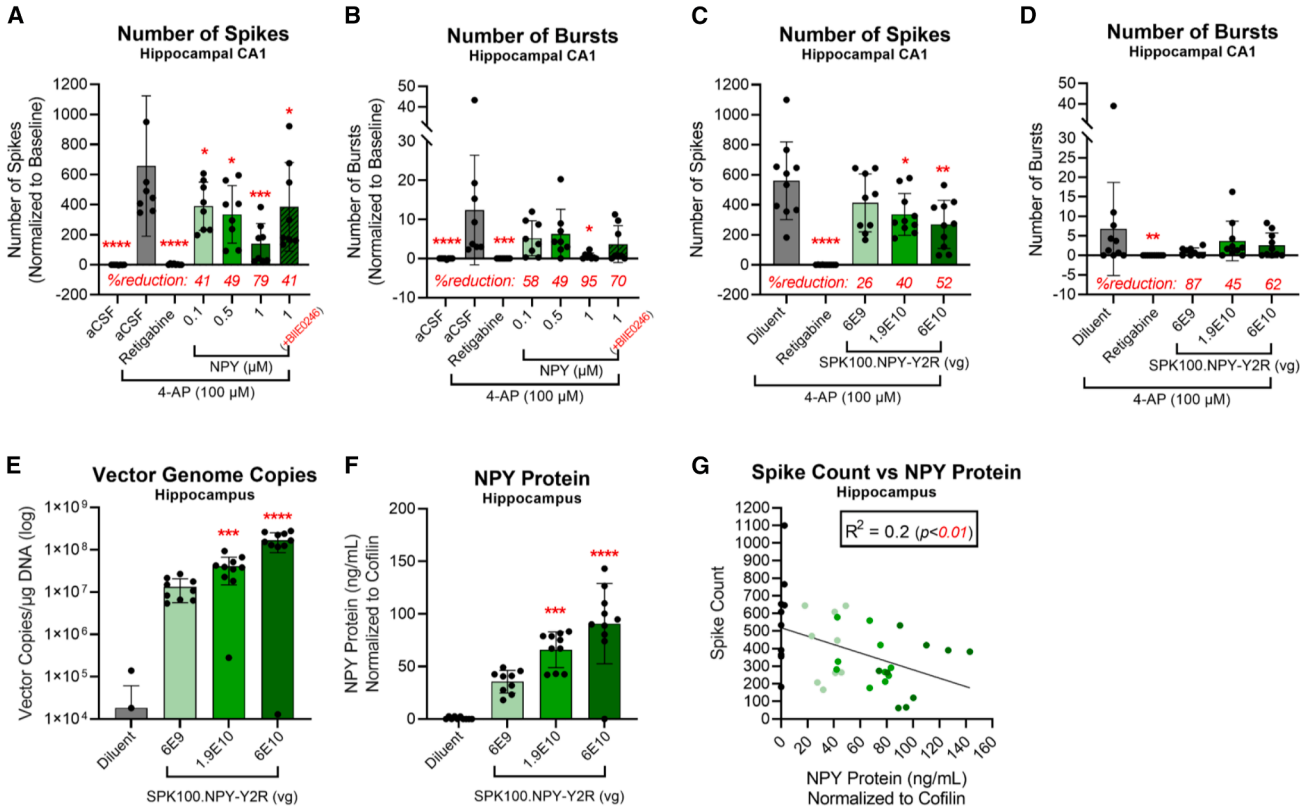

Figure 2. NPY peptide or SPK100.NPY-Y2R reduce 4-AP-evoked activity in *ex vivo* slices of mouse hippocampus

(A) Bath application of NPY (0.1, 0.5, and 1 μM) dose dependently and significantly reduced the number of spikes in the hippocampal CA1 subfield evoked by 4-AP (*ex vivo* microelectrode [MEA] array recordings). The inhibitory effects of NPY at 1 μM were partially attenuated by addition of a Y2 receptor antagonist, BIIE0246, at 0.6 μM ($p < 0.0001$). Unpaired, t test between 1 μM NPY and 1 μM NPY + BIIE0246 groups, $p = 0.05$. (B) Bath application of NPY significantly reduced the number of 4-AP-evoked bursts detected by MEA in the hippocampal CA1 at 1 μM (Kruskal-Wallis, $p < 0.0001$). Unpaired, t test between 1 μM NPY and 1 μM NPY + BIIE0246 groups, $p = 0.09$. (C) Intrahippocampal delivery of SPK100.NPY-Y2R 3 weeks prior to *ex vivo* MEA recordings dose dependently and significantly (1.9×10^{10} and 6×10^{10} vg per mouse) reduced the number of 4-AP-evoked spikes detected in the hippocampal CA1 ($p < 0.0001$), and (D) trended toward reduced burst activity (Kruskal-Wallis, $p = 0.005$). (E) Vector genome copies in *ex vivo* hippocampal slices used for MEA recordings reflected a dose dependent and significant increase in vector copies in SPK100.NPY-Y2R-treated hippocampi versus diluent-treated controls (Kruskal-Wallis, $p < 0.0001$). Data are represented as vector copies per μg of DNA on a log-scale. (F) NPY protein abundance was also dose dependently and significantly increased in *ex vivo* hippocampal slices used for MEA recordings compared with diluent-treated controls (Kruskal-Wallis, $p < 0.0001$). One animal in the high dose group (6×10^{10} vg per animal) reflected minimal vector copies and NPY protein abundance in the hippocampus. (G) There was a significant, negative correlation between neuronal spiking activity (count) in the hippocampal CA1 and the abundance of NPY protein (ng mL^{-1}) in *ex vivo* hippocampal slices (simple linear regression, $R^2 = 0.2$, $p = 0.0054$). All data: one-way ANOVA followed by Holm-Šídák's multiple comparisons test referenced to aCSF/Diluent + 4-AP (100 μM) conditions unless otherwise noted; Dunn's multiple comparisons test used with Kruskal-Wallis (*$p < 0.05$, **$p < 0.01$, ***$p < 0.001$, ****$p < 0.0001$). Data are represented as mean ± standard deviation. For NPY peptide experiments: $n = 8$ slices per group (1–3 slices per mouse from 3 to 5 mice). For SPK100.NPY-Y2R experiments: $n = 10$ slices per group (1 slice per mouse from 10 mice). aCSF, artificial cerebrospinal fluid.

hypothalamic neurons, we measured any effects of SPK100.NPY-Y2R treatment on body weight.[49–51] Notably, mice receiving bilateral intrahippocampal delivery of SPK100.NPY-Y2R showed a dose-dependent and significant increase in body weight by 21 days post-treatment when compared with diluent-treated controls (Figure S2H).

Intrahippocampal SPK100.NPY-Y2R treatment reduces seizure severity and duration in a rat model of epilepsy

Previous work demonstrated the seizure-suppressant effects of AAV.NPY-Y2R in rats using intrahippocampal delivery with an AAV1 capsid serotype.[36] To maximize hippocampal coverage and treatment efficacy, we compared the resultant vector biodistribution and NPY protein abundance after intrahippocampal delivery of either AAV1.NPY, AAV9.NPY, or AAV-Spark100.NPY vectors in mice, and found that both AAV9 and AAV-Spark100 conferred improved biodistribution when compared with AAV1 (Figures S3 and S4). Specifically, AAV9 and AAV-Spark100 demonstrated higher and more consistent transduction of cells through the dentate gyrus, CA3, CA2, and CA1 hippocampal subfields compared with AAV1 when measured by RNAscope *in situ* hybridization (Figures S4A and S4B). These data, as well as the fact that the AAV-Spark100 capsid is on our manufacturing platform, motivated

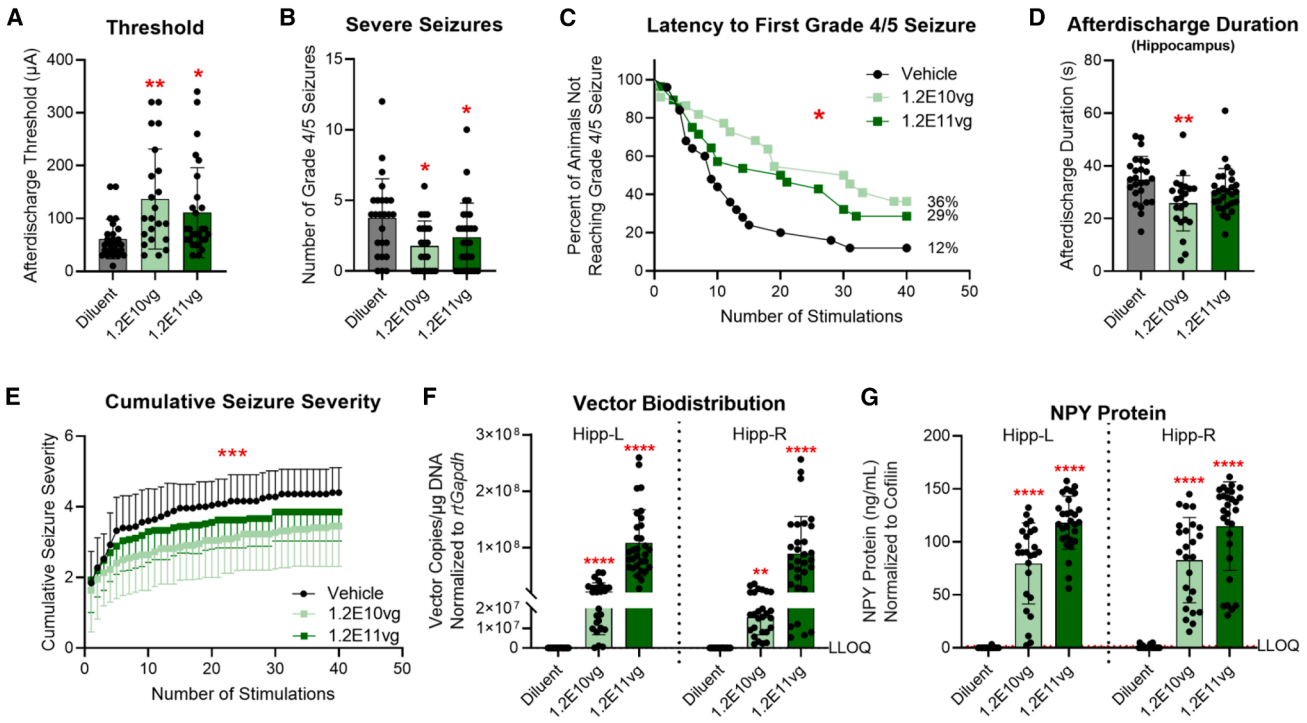

Figure 3. Intrahippocampal delivery of SPK100.NPY-Y2R reduces seizure severity and duration in the rat, *in vivo* rapid kindling model of epilepsy

(A) The threshold current (μA) required to elicit an EEG afterdischarge of ≥5 s recorded from the hippocampal depth electrode was significantly greater, on average, in SPK100.NPY-Y2R-treated rats versus diluent-treated controls ($p = 0.0036$). (B) The total number of Racine grade 4 or 5 behavioral seizures (severe seizures) over all 40 kindling stimulations was significantly lower, on average, in SPK100.NPY-Y2R-treated rats compared with diluent-treated controls ($p = 0.016$). (C) The latency to the first Racine grade 4 or 5 behavioral seizure event was significantly increased in SPK100.NPY-Y2R-treated rats versus diluent-treated controls (long-rank [Mantel-Cox], $p = 0.025$). (D) The afterdischarge duration (seconds) measured from the hippocampal depth electrode after each 400 μA stimulation, and averaged across all 40 stimulations, was lower in SPK100.NPY-Y2R-treated rats compared with diluent-treated controls ($p = 0.0067$). (E) The cumulative seizure severity over all 40 kindling stimulations was significantly lower in SPK100.NPY-Y2R rats compared with diluent-treated controls (two-way, repeated measures ANOVA: effect of stimulation, $p < 0.0001$, effect of treatment, $p < 0.001$, effect of interaction, $p = 0.03$). (F) Vector genome copies (represented as per μg of DNA and normalized to rat *Gapdh*) detected across both left and right hippocampi of SPK100.NPY-Y2R-treated rats were dose dependently and significantly increased over diluent-treated controls (Kruskal-Wallis, $p < 0.0001$). (G) NPY protein abundance was significantly increased in SPK100.NPY-Y2R-treated rat hippocampi (left and right hemispheres) compared with diluent-treated controls (represented as ng mL^{-1} normalized to Cofilin protein levels) (Kruskal-Wallis, $p < 0.0001$). All data: one-way ANOVA followed by Holm-Šídák's multiple comparisons test referenced to Diluent unless otherwise noted; Dunn's multiple comparisons test used with Kruskal-Wallis (*$p < 0.05$, **$p < 0.01$, ***$p < 0.001$, ****$p < 0.0001$). All data are represented as mean ± standard deviation. Diluent: $n = 25$ rats; SPK100.NPY-Y2R (1.2×10^{10} vg per animal): $n = 22$ rats; SPK100.NPY-Y2R (1.2×10^{11} vg per animal): $N = 28$ rats. LLOQ, lower limit of quantification.

our continued investigation of the AAV-Spark100 capsid to deliver our payload to the hippocampus *in vivo*.

We next sought to determine the anti-seizure potential of SPK100.NPY-Y2R treatment *in vivo*. We employed the well-established rat rapid kindling model to track the progression of seizures induced by electrical stimulation of the hippocampus, providing a reliable measure of seizure development and severity.[52,53] In this paradigm, rats receive 40 suprathreshold (400 μA) current stimulations into the ventral hippocampus, gradually developing longer and more behaviorally severe seizures. To test the anti-seizure effects of our therapy, adult male rats received bilateral, intrahippocampal delivery of either SPK100.NPY-Y2R at two doses (1.2×10^{10} or 1.2×10^{11} vg total per rat) or vehicle (vector diluent), 4 weeks before kindling.

Prior to initiating the rapid kindling procedure, the threshold current (the current required to elicit an EEG afterdischarge of ≥5 s measured from the hippocampal depth electrode) was measured for each animal. The current (μA) required to induce a ≥5 s afterdischarge in the hippocampus was significantly higher in SPK100.NPY-Y2R-treated rats (at both doses) compared with diluent-treated controls (Figure 3A).

During the rapid kindling period, SPK100.NPY-Y2R-treated animals exhibited a significant reduction in the number of severe, tonic-clonic (Racine grade 4 or 5) seizures (Figure 3B). The latency to the first severe seizure event was increased compared with diluent-treated controls (Figure 3C). Correspondingly, the average afterdischarge durations over all 40 stimulations measured by the hippocampal depth electrode and surface electrodes (electroencephalogram

[EEG]) were significantly reduced in SPK100.NPY-Y2R-treated animals versus diluent-treated controls. However, this reduction was only statistically significant in the 1.2×10^{10} vg per animal dose group (Figures 3D and S5B). Furthermore, the cumulative seizure severity measured over all 40 stimulations was significantly reduced in SPK100.NPY-Y2R-treated rats versus diluent-treated controls (Figure 3E). No significant difference was found between the two doses of SPK100.NPY-Y2R in any of the investigated outcome parameters.

Bioanalysis of micro-dissected hippocampal brain tissues from all rats after the study confirmed a dose-dependent and significant increase in vector genome copies in SPK100.NPY-Y2R-treated animals compared with diluent-treated controls (Figures 3F and S5C). NPY protein abundance was also significantly increased in both hippocampi of SPK100.NPY-Y2R-treated rats compared with diluent-treated controls (Figures 3G and S5D). However, a plateau in NPY protein abundance was observed once a certain threshold of SPK100.NPY-Y2R vector copies was reached in the hippocampus (Figure S5E). Body weight was slightly, but significantly, increased in the 1.2×10^{10} vg per animal dose group of SPK100.NPY-Y2R over diluent-treated controls (Figure S5A), mirroring the findings reported above in mice receiving bilateral, intrahippocampal delivery of SPK100.NPY-Y2R. Collectively, these results support the idea that AAV-mediated NPY and Y2 overexpression in the hippocampus can reduce seizure severity and burden in a focal model of epilepsy.

The electrical kindling model is limited by the evoked nature of each seizure event compared with models presenting with spontaneous seizures. Parallel experiments using AAV9-mediated delivery of our same, dual construct (AAV9.NPY-Y2R), showed that bilateral, intrahippocampal AAV.NPY-Y2R (5×10^{10} vg total per animal) is also able to significantly reduce the number of spontaneous seizures and delay seizure onset in a genetic model of epilepsy (synapsin triple knockout [TKO] mice; Figures S6A–S6C). In this model, deletion of the three murine synapsin genes (*Syn1*, *Syn2*, and *Syn3*) results in an increased propensity to develop spontaneous seizures that arise between 40 and 120 days of life.[54] Importantly, we confirmed overexpression of both NPY and Y2R proteins in the hippocampus after intraparenchymal delivery of AAV9.NPY-Y2R at this dose (Figures S7A and S7B). In line with the results reported above for mice receiving intrahippocampal SPK100.NPY-Y2R (Figure S2H), there was also a significant increase in body weight in AAV9.NPY-Y2R-receiving mice (Figure S6D). These additional data further support that AAV-mediated NPY and Y2 overexpression in the hippocampus can suppress seizures.

Successful SPK100.NPY-Y2R biodistribution in *Papio hamadryas* hippocampus following MRI-guided CED

Building upon the efficacy demonstrated in rodent models, we aimed to evaluate the feasibility of SPK100.NPY-Y2R delivery in non-human primates to further bridge the translational gap toward human applications. Non-human primates, due to their larger brains and more complex anatomy, offer a critical step forward in determining the suitability of this approach for clinical application. We aimed to characterize vector biodistribution and transduction in non-human primate brain after intraparenchymal delivery to inform future human trials. We also extended our capsid comparison initially performed in mice (Figures S3 and S4) to compare AAV9- versus AAV-Spark100-mediated delivery of our payload to the non-human primate hippocampus. SPK100.NPY-Y2R or AAV9.NPY-Y2R (1×10^{11} vg mL^{-1}) was unilaterally infused into the right hippocampus of adult, *Papio hamadryas* (baboon) females via magnetic resonance imaging (MRI)-guided convection enhanced delivery (CED) (Figure 4A). Baboons were chosen due to their larger hippocampal volume and closer anatomical similarity to humans compared with other non-human primates commonly used in biomedical research, making them a more suitable model for evaluating the delivery and biodistribution of the therapy.[55,56] Importantly, all animals were screened for the presence of antibodies to the AAV-Spark100 and AAV9 capsids prior to dosing and were considered seronegative with serum neutralizing antibody titers lower than 1:1 at baseline (see materials and methods for details). Each animal was injected with approximately 200 μL into the right hippocampus, corresponding to a total of 2×10^{10} vg, except for one animal that received 142 μL due to smaller hippocampal size (Table 1). The left hippocampus was administered SPK100.dTomato or AAV9.dTomato using the same infusion protocol and the same capsid as on the right hemisphere (Figure 4A). The bilateral administrations resulted in an average coverage of around 72% based on the MRI contrast agent (ProHance) volume of distribution to hippocampal volume (Figure 4A; Table 1). Overall, the MRI-guided CED targeting of the hippocampus of baboons was quantitatively successful.

No mortality or adverse events were reported for any animals throughout the study, including during cage-side neurological function assessments measured up to the 1-month post-treatment endpoint. Overall, no significant changes in body weight (defined as weight change exceeding 20%) were observed from baseline to necropsy, and all animals were deemed healthy per veterinarian-performed physical exam. Analysis of NPY protein abundance from cerebrospinal fluid (CSF) and blood plasma samples showed no significant change in NPY abundance in SPK100.NPY-Y2R-treated baboons when compared with pre-surgery baseline levels, but did reflect an increase in NPY abundance in the CSF of AAV9.NPY-Y2R-treated animals, specifically (Figures S8A and S8B). Each animal ($n = 6$) was humanely euthanized 1-month post-infusion (±3 days), and brain tissues were collected for evaluation of vector biodistribution and NPY protein abundance.

Histological analysis of brain tissues revealed NPY protein in the targeted hippocampus of both SPK100.NPY-Y2R- and AAV9.NPY-Y2R-treated baboons, particularly in the body (intermediate hippocampus) and head (anterior hippocampus) of the structure (Figures 4B and S9). Furthermore, vector genome copies and NPY protein were enriched in the right hippocampus 1 month after AAV9/SPK100.NPY-Y2R infusion compared with non-targeted

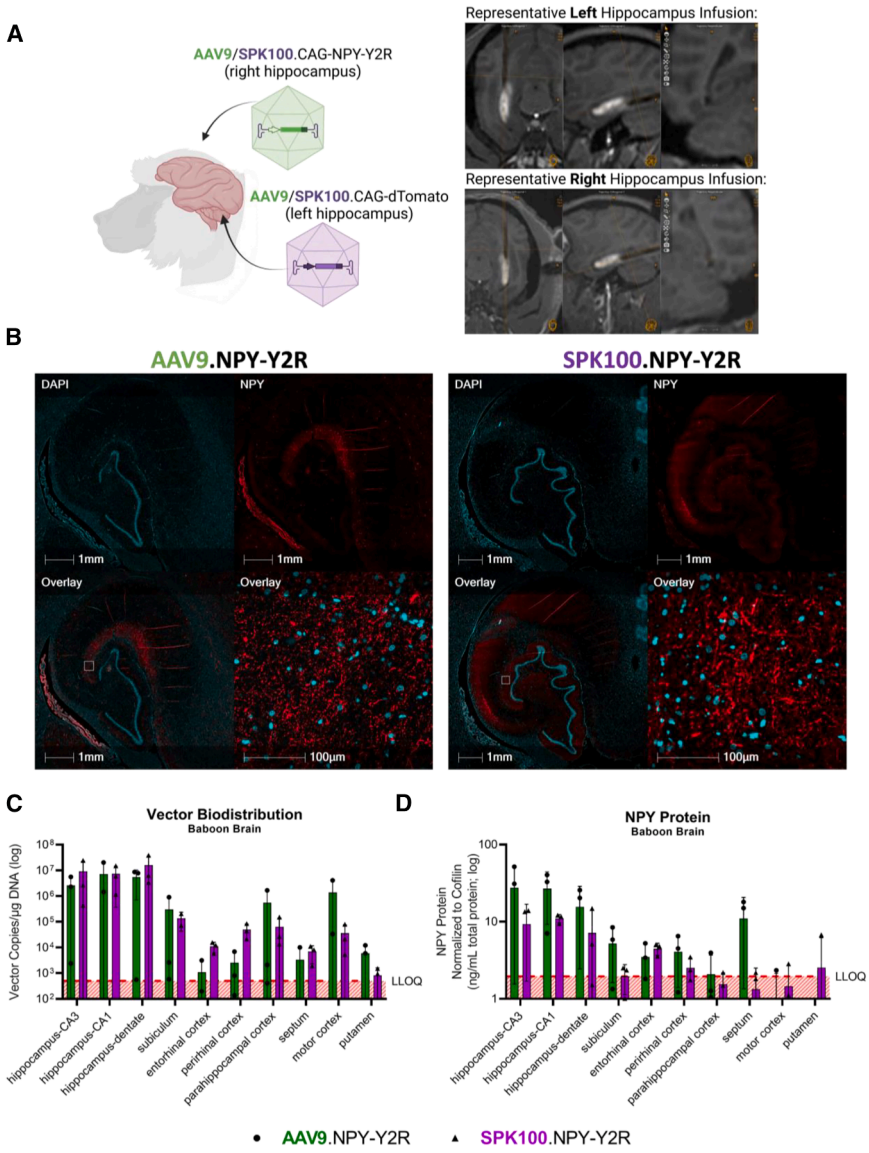

Figure 4. MRI-guided convection enhanced delivery of SPK100.NPY-Y2R results in successful coverage and vector biodistribution of baboon hippocampus

(A) Left: schematic demonstrating the study approach for bilateral, hippocampal delivery of AAV-Spark100 or AAV9 vectors. Right: representative MRI contrast agent (ProHance) signal from the left (top) and right (bottom) hippocampus of one, representative baboon demonstrating infusion coverage upon hippocampal intraparenchymal infusion using MRI-guided convection enhanced delivery. (B) Immunohistochemistry of NPY protein (red) demonstrating expression in targeted, right hippocampus of a representative AAV9.NPY-Y2R-receiving (left) and SPK100.NPY-Y2R-receiving (right) baboon. DAPI stain (nuclei) is depicted in cyan. (C) Vector genome copies detected across various, micro-dissected brain regions of the right hemisphere of each baboon 1 month after infusion reflect comparable vector biodistribution between SPK100.NPY-Y2R- and AAV9.NPY-Y2R-treated baboons (mixed-effects analysis, ns). Data are represented as vector copies per µg of DNA on a log-scale. (D) NPY protein abundance across the same micro-dissected brain regions analyzed for vector genome copies 1 month after infusion was not significantly different between SPK100.NPY-Y2R- and AAV9.NPY-Y2-treated baboons (mixed-effects analysis, ns). Data are represented as ng mL^{-1} of NPY normalized to Cofilin protein on a log-scale. One baboon receiving AAV9.NPY-Y2R into the right hippocampus had suboptimal delivery/targeting noted during the surgery based on contrast agent visualization, with minimal vector copies and NPY protein abundance detected in the hippocampus. Green: AAV9.NPY-Y2R; Purple: SPK100.NPY-Y2R. Data are represented as mean ± standard deviation. *n* = 3 *Papio hamadryas* females per group (*n* = 6 animals total). LLOQ, lower limit of quantification.

brain regions (Figures 4C, 4D, S8C, and S8D). Specifically, vector genome copies and NPY protein abundance were highest in brain tissue samples collected from the hippocampal CA1, CA3, and dentate gyrus subfields, with no significant difference between AAV9- and AAV-Spark100-treated animals (although the number of animals in this initial study was limited) (Figures 4C, 4D, S8C, and S8D). In contrast, NPY protein was nearly undetectable in brain areas distal to the infusion site, such as motor cortex and putamen (Figures 4C, 4D, S8C, and S8D). One baboon receiving AAV9.NPY-Y2R into the right hippocampus had suboptimal delivery/targeting noted during the surgery based on contrast agent visualization, with minimal vector copies and NPY protein abundance detected in the hippocampus (Figures 4C, 4D, S8C, and S8D). Overall, the surgery with AAV administration to the hippocampus was successful in achieving vector genome enrichment in the target brain region and was well tolerated by the baboons. These data also reflect that our platform capsid, AAV-Spark100, provides comparable vector biodistribution to AAV9 in the baboon hippocampus. Collectively, the biodistribution pattern of SPK100.NPY-Y2R in the non-human primate brain is encouraging for further translational research with this approach.

Taken together, the results from both rodent and baboon studies provide compelling evidence that SPK100.NPY-Y2R can be delivered safely and effectively into the hippocampus. The successful transition from rodent to non-human primate models positions this approach as a strong candidate for clinical development in humans.

DISCUSSION

Overall, our study presents strong new evidence supporting the anti-seizure effects of the newly developed AAV vector, SPK100.NPY-Y2R, which mediates overexpression of NPY and Y2R across several relevant preclinical models of epilepsy. We leveraged our previously

Table 1. Hippocampal volumes of infusion and distribution in *Papio hamadryas* hippocampus

		Infusate delivered (μL)		Intrahippocampal ProHance distribution (mm^3)		Hippocampus coverage (%)	
Animal	Capsid (AAV.NPY-Y2R)	Left	Right	Left	Right	Left	Right
1	AAV-Spark100	202	202	470	537	69.7	74.3
2	AAV-Spark100	202	198	535	488	73.0	71.2
3	AAV-Spark100	142	202	430	424	70.0	70.2
4	AAV9	202	202	476	443	68.9	63.7
5	AAV9	202	202	499	458	78.6	78.6
6	AAV9	202	202	513	499	72.7	69.8

The left hippocampus was injected with AAV9/SPK100.dTomato and the right hippocampus with AAV9/SPK100.NPY-Y2R.

described construct expressing both NPY and Y2 (originally encapsulated in AAV1) in combination with a bioengineered capsid, AAV-Spark100, to significantly enhance our therapeutic biodistribution.[26] We also validate *in vitro*, *ex vivo*, and *in vivo* models suitable for testing AAV-based gene therapies, particularly for TLE. Importantly, we demonstrate effective biodistribution of our new vector to the hippocampus in a non-human primate brain, a critical step for translating this therapy to human clinical trials.

Preclinical assays for validation of anti-seizure effects of AAV gene therapies

Numerous *in vitro* and *in vivo* models of epilepsy have been developed and used for screening of various anti-seizure therapies.[57,58] However, many *in vivo* epilepsy models which are ideal for early-stage candidate screening tend to induce generalized seizures that respond to systemically delivered small molecules. This limits their usefulness in assessing the efficacy of locally targeted gene therapies designed for treating focal seizures, such as in TLE.[59] Furthermore, the advancement of gene therapies for epilepsy has been hindered by the inherently high variability of many seizure models and scarcity of models that accurately replicate human pathophysiology.[60] Therefore, in this study, we sought to develop a reliable road map, from *in vitro* through *in vivo*, for pre-clinical evaluation of gene therapy vectors specifically aimed at modulating neuronal activity for the treatment of TLE. This work adds to the current landscape of gene therapies in-development for TLE, including a gene therapy vector sponsored by UniQure currently in clinical trial (ClinicalTrials.gov NCT06063850).[61,62]

The ability of several AAV capsids to effectively transduce cultured primary neurons makes calcium imaging an attractive and high-throughput *in vitro* screening system for therapies that effectively modulate neuronal activity.[63] The *in vitro* method described in this report provides a valuable, long-term activity assay based on primary cortical neurons, allowing for the assessment of payloads that modulate neuronal activity over extended periods. Indeed, our present results demonstrate that AAV-mediated overexpression of NPY and Y2R in this system significantly reduces multiple Ca^{2+}-based readouts of spontaneous neuronal activity over nearly 1 month *in vitro*. There was a reduction in cell viability of primary cortical neurons *in vitro* after transduction with SPK100.NPY-Y2R (Figure S1B). However, the doses applied in our proof-of-concept *in vitro* experiments (up to 5×10^6 vg per cell) were fairly high and may not accurately model the vector genomes per cell ultimately delivered *in vivo* using our intraparenchymal route of administration. Notably, we did not observe any behavioral adverse events in rodents or non-human primates receiving intrahippocampal delivery of SPK100.NPY-Y2R at our tested doses *in vivo*. There were also no neurological phenotypes reported for any non-human primates during cage-side neurological function assessments measured up to the 1-month post-treatment endpoint. Despite this, it remains critical to establish a safety window for SPK100.NPY-Y2R, particularly within an efficacious dose range and using the intended route of administration/delivery device.

Furthermore, our efforts in bridging *ex vivo* and *in vivo* TLE models for assessing gene therapy efficacy underscores the importance of focusing seizure suppression testing on specific, focal regions, in this case the hippocampus. *Ex vivo*, the spatial resolution and sensitivity of MEA recording systems can be utilized to gain detailed insights into population-level neural activity within specific circuits of interest.[64] In this study, we report that SPK100.NPY-Y2R treatment significantly reduces population activity in hippocampal CA1 neurons, which contain the primary output projections from the hippocampus, during 4-AP evoked burst firing. These findings support the potential of AAV-mediated NPY and Y2R overexpression in the hippocampus to reduce evoked, seizure-like activity within this circuit, and possibly limit seizure spread beyond the site of origin in TLE. In line with our results, it has been reported that epileptiform activity induction can be suppressed using bath-applied NPY.[24,65,66]

In our *in vivo* TLE model, the ventral hippocampus of rats was kindled by electrical stimulation, successfully triggering seizures and hippocampal EEG discharges. These progressive seizures were effectively counteracted by local overexpression of NPY and Y2R in the hippocampus. It is nonetheless important to highlight that the rapid kindling model applied in this study is limited by the evoked nature of each seizure event, as well as the number of severe,

generalized seizures elicited in rapid succession. Given our localized therapeutic delivery, we leveraged the electrical kindling model using stimulating electrodes implanted directly into the ventral hippocampus for our initial *in vivo* efficacy experiments. In parallel, we report that AAV9-mediated delivery of our same construct significantly reduces seizures in a genetic model presenting with spontaneous seizures (synapsin TKO mice; Figure S6). However, it will be important to expand upon these findings, particularly in future dose-finding studies, by specifically screening SPK100.NPY-Y2R in additional seizure models such as those presenting with spontaneous seizure events (e.g., kainate- or pilocarpine-induced post-status epilepticus models). Thus, although a combination of *ex vivo* and *in vivo* models strongly suggests that hippocampal overexpression of NPY and Y2R is sufficient to suppress seizures in TLE, differences in ictogenesis compared with human patients make prediction of the extent of clinical efficacy from rodent to human challenging.

Of note, there was no significant difference in seizure phenotypes measured in the rat kindling model between the two doses of SPK100.NPY-Y2R administered in this study (1.2×10^{10} and 1.2×10^{11} vg per animal). Interestingly, there was also a plateau in the NPY protein abundance detected in the hippocampus of rats receiving intrahippocampal SPK100.NPY-Y2R, with no significant increase in NPY protein (despite a dose-dependent increase in vector copies) between the lower and higher dose groups (Figures 3G and S5E). This may reflect a ceiling in transgene overexpression achievable in the rodent hippocampus using this route of administration, perhaps as a result of the high doses delivered in this initial efficacy study. This limits the interpretation of a dose-response relationship between the administered viral doses and any seizure phenotype outcome in this model. It will be important to expand upon these findings in future dose finding studies, including at lower doses, to properly evaluate a dose-response relationship and establish a minimal effective dose for SPK100.NPY-Y2R.

Leveraging the endogenous NPY-Y2R signaling pathway as a therapeutic approach for focal epilepsy

The endogenous neuropeptide signaling system presents an attractive target for modulating neuronal activity in a disease context such as epilepsy.[67] Endogenous neuropeptides like NPY are typically released by local interneurons to modulate glutamatergic transmission of principal cells within specific circuits such as the hippocampus.[68] However, the loss and dysfunction of interneurons has been linked to epileptogenesis and the subsequent occurrence of seizures.[69] Boosting of the NPY-Y2R signaling system through gene therapy-mediated overexpression harnesses an innate mechanism for regulating excitatory transmission in the hippocampus, even in a dysregulated environment. Our rationale for including both NPY and Y2R in our vector was motivated by previous reports that have supported a role for Y2R in mediating the seizure-suppressant effects of NPY by pre-synaptically inhibiting glutamate release.[24,25] Y2R agonists mimic the NPY-mediated inhibition of glutamatergic transmission and epileptiform discharges in two different slice models of TLE (stimulus train-induced bursting and 0-Mg^{2+}).[24] Similarly, the Y2R-specific inhibitor (BIIE0246) attenuates the inhibitory effects of NPY on evoked burst firing in hippocampal slices of both rodents and humans.[13,18,26,66] Finally, Y2R binding is upregulated in rodents after seizures as well as in human patients with TLE.[27,28] In contrast, NPY action at Y1 receptors has been reported to facilitate seizure activity.[38–40] Therefore, our dual NPY-Y2R approach aims to boost Y2R-mediated signaling of NPY to confer seizure suppression. Additional data have more directly evaluated the seizure-suppressant effects of NPY or Y2R alone or NPY in combination with Y2R. Overexpression of Y2R in the hippocampus of rats using rAAV vectors is sufficient to reduce seizures in two distinct rodent models of TLE: electrical kindling and the kainate-induced seizures.[35] Importantly, co-administration of rAAV-Y2R with rAAV-NPY into the rat hippocampus was reported to confer an additive, anti-seizure effect beyond rAAV-Y2R-only in the same electrical kindling model of seizures.[35] These findings support the seizure-suppressant effects of Y2R overexpression alone and reinforce the rationale for pursuing a dual NPY-Y2R therapy for treatment of hippocampal seizures. In fact, AAV-mediated overexpression of NPY and Y2R has been shown to decrease glutamate release in nearby synapses that are not actively releasing NPY during high-frequency stimulation in the CA1 area of the hippocampus.[10] Supporting this, several studies have demonstrated the anti-seizure effects of AAV-mediated overexpression of NPY and/or Y2R in various rodent models of epilepsy.[26,35–37] It is important to highlight that one of these studies demonstrated a reduction in the number of spontaneous recurrent seizures in already epileptic rats after unilateral intrahippocampal delivery of an AAV1.NPY-Y2R vector.[36]

Therefore, our working hypothesis is that the activity-dependent ("on-demand") release of NPY overexpressed by our vector is sufficient to reduce pre-synaptic release of glutamate during prolonged, high-frequency burst firing of neurons to attenuate aberrant activity. It is possible that co-expression of NPY and Y2R in the same cells may lead to auto-inhibition of NPY release (as has been described for sympathetic neurons).[70] While we cannot exclude this possibility for hippocampal neurons, it is important to note that the mechanisms and timing of neuropeptide release, signaling, and reuptake differ from those of traditional neurotransmitters such as glutamate. For example, neuropeptides can be released extra-synaptically, signal via volume transmission, and are more slowly removed from the extracellular space due to the lack of specialized transporters.[71] A combination of these factors may contribute to the relatively long-lasting effects of neuropeptides compared with classical neurotransmitters, and in this case, may allow for attenuated glutamate release by NPY despite any auto-inhibition. Importantly, baseline excitatory synaptic transmission in the hippocampal CA1 is reportedly not affected by AAV-mediated overexpression of NPY and Y2R, supporting the hypothesis of an on-demand, autoregulatory loop for NPY release and action.[26] The results of this current study align with these findings, wherein SPK100.NPY-Y2R treatment did not impact spontaneous spiking or bursting activity at baseline in *ex vivo* mouse hippocampal slices compared with vehicle-treated controls (Figures S2E and S2F). Additionally, no overt neurological

abnormalities were observed in adult baboons up to 1 month after receiving unilateral, intrahippocampal infusion of SPK100. NPY-Y2R.

The relative stoichiometry and absolute levels of NPY and Y2R proteins required for optimal seizure-suppression remains uncertain, particularly within specific cell types of the hippocampus. Our rationale in selecting a strong, ubiquitous promoter (CAG) was driven by a desire to maximize our vector potency and efficacy. In future experiments, it would be informative to evaluate efficacy and potency after restricting NPY and/or Y2R expression using cell-type-specific promoters. Importantly, we demonstrate that our vector is capable of overexpressing both the NPY and Y2R transgene proteins in the targeted hippocampus (Figure S7). In future studies, it will be informative to interrogate the exact stoichiometry of NPY and Y2R proteins necessary for therapeutic efficacy in the hippocampus, as well as the specific cell types necessary to mediate seizure-suppressant effects. Notably, a recent publication has demonstrated that lentiviral-mediated delivery and expression of NPY and Y2R restricted to excitatory neurons of the hippocampus (CaMKII promoter) is sufficient to reduce seizures in a genetic model of epilepsy, the synapsin TKO mouse.[72]

In addition to its role in the hippocampus, NPY is a well-established orexigenic factor that influences feeding behavior and body weight through its actions on hypothalamic neurons.[49–51] Specifically, AAV-mediated NPY overexpression in the dorsomedial hypothalamus and paraventricular nucleus of the hypothalamus is reported to result in increased food intake and weight gain.[73,74] In this study, we report that unilateral, intrahippocampal infusion of SPK100. NPY-Y2R into baboons did not result in significant weight gain 1 month after delivery, in contrast with what was observed upon bilateral delivery in rodents. This discrepancy may be due to several factors, including differences in access to food (rodents, but not baboons, had *ad libitum* access), unilateral versus bilateral NPY and Y2R administration, differences in SPK100.NPY-Y2R vector biodistribution between rodents and primates, differences in extrahippocampal infusion leakage given the different surgical approaches in rodents versus baboons, anatomical differences in subcortical structures (such as the relative proximity of the hypothalamus to the hippocampus) between the two species, or the impact of intrahippocampal SPK100.NPY-Y2R dose on weight gain. We had previously not observed weight gain in rats following bilateral or unilateral intrahippocampal administration of AAV1.NPY-Y2R.[26,75] In addition to differences in AAV serotype, other significant modifications in the present study were the number of infusion sites and total volume administered, resulting in twice the volume compared with what was used previously. Moreover, the larger relative weight gain seen in mice versus rats reported here may be explained by the larger volume of infusate per volume of hippocampus administered in the mouse versus rat. It is conceivable that the high volumes used in rodents in the present study led to vector overspill into adjacent brain regions, thus contributing to exposing the hypothalamus to exogenous NPY and possibly triggering an orexigenic effect. These results highlight the need to model potential on- and off-target effects of NPY-Y2R overexpression using the same doses and surgical delivery methods proposed for human use.

Successful delivery and biodistribution of AAV-Spark100 capsid to *Papio hamadryas* hippocampus

Non-human primates (NHPs) serve as an effective test system for nonclinical therapeutic biodistribution and toxicity studies accepted by regulatory agencies.[76–78] NHPs have been shown to produce transgene expression levels comparable to those observed in humans in other AAV-based gene therapy studies. Importantly, NHPs can model the production of neutralizing antibodies to both AAV capsid proteins and transgene proteins, which can substantially alter vector biodistribution and subsequent efficacy; NHPs can thereby provide biodistribution and expression data that are translatable for future developmental studies.[76–79] We hypothesized that *Papio hamadryas* (baboon) could be an advantageous model for evaluating intraparenchymal surgical delivery methods and vector biodistribution, given their larger brain size compared with other NHPs commonly used in biomedical research (e.g., a 12 kilogram baboon has a median brain mass of 140–150 g).[80] Baboons also have favorable subcortical brain structures, with the hippocampus being 2- to 3-fold larger in volume than other Old World NHP species (e.g., *Macaca fasciularis*).[55,81] Additionally, the baboon hippocampus is only 2- to 3-fold smaller in volume than that of the human, allowing for the scaling up of AAV doses based on volume.[56] This larger neuroanatomical target makes baboons a valuable model for studying delivery methods and therapeutic effects. Although less common, baboons are also an accepted test system for nonclinical biodistribution and toxicity testing by regulatory agencies, including gene therapy.[76–78,82]

This study is, to our knowledge, the first to report successful MRI-guided, CED of AAV into the hippocampus of baboons. No adverse events or premature mortality were observed in any of the animals included in this study. Cage-side neurological assessments up to 1-month post-surgery showed no overt signs of neurological impairment, and no unexpected gross findings or lesions were reported at necropsy. Bioanalysis revealed an enrichment of vector copy numbers and NPY protein in the targeted hippocampus, particularly the CA1, CA3, and dentate gyrus subfields, with minimal spread to non-targeted brain areas. Vector genomes outside the hippocampus were largely confined to hippocampal-associated projections including subiculum, entorhinal cortex, para-hippocampal cortex, and perirhinal cortex at about 100 to 1,000-fold lower compared with the hippocampus, with NPY protein abundance at or below the limit of detection. Our present data also reflect no significant difference in vector biodistribution in the brain between AAV9. NPY-Y2R- and SPK100.NPY-Y2R-treated animals, providing encouraging evidence that our platform AAV-Spark100 capsid can be suitable for brain-directed gene therapies.

Bridging an NPY-Y2R gene therapy to mesial TLE patients

Several alternative gene therapies approaches are being explored and developed for the treatment of refractory epilepsy, each targeting

different mechanisms to reduce neuronal excitability. These include overexpression of an engineered potassium channel which dampens excitability by promoting a prolonged influx of potassium, stabilizing neural activity.[83] Another strategy, currently in clinical trial as mentioned above, leverages two anti-*GRIK2* micro-RNAs to lower the levels of a kainate receptor subunit in the hippocampus and reduce excessive excitatory signaling during seizures.[61] Finally, overexpression of the neuropeptide dynorphin has also shown promise in preclinical models for its potential to mitigate seizures.[84] The dual-NPY/Y2R strategy described here offers distinct advantages, notably in that the neuropeptide is demonstrated to release and signal on demand, potentially reducing adverse effects associated with continuous activity modulation.[26] Furthermore, boosting the innate NPY-Y2R signaling pathway over NPY action on other endogenous receptors such as Y1 can lead to a more effective therapeutic action. In the context of epilepsy therapeutics more broadly, focal overexpression of NPY and Y2R holds some advantages over existing surgical methods available for patients with refractory seizures (e.g., laser interstitial thermal therapy, surgical resection, or stereo EEG-guided radiofrequency thermocoagulation). The most prominent advantage is the less invasive nature of the administration compared with *in situ* resection or coagulation, including possible treatment and preservation of the eloquent cortex.

NPY abundance in the baboon CA1 and CA3 reached approximately 10 ng mL^{-1} total protein (Figure 4D). This is significantly lower than the 80–120 ng mL^{-1} total protein range of NPY protein observed in rats receiving intrahippocampal delivery of SPK100.NPY-Y2R (Figure 3G), likely due to the relatively lower dose per tissue volume that was administered to the baboons. Given the non-linear relationship between vector copy numbers and resultant NPY protein abundance observed in the rats of this study (Figure S5E), it remains difficult to scale effective dose from the rat kindling model presented here to the human situation based on structure volume alone. Further dose-finding in the baboons using the device and route of administration intended for clinical use will guide the extrapolation to human patients. Direct targeting to the hippocampus in human mTLE patients may also involve a more individualized approach. For example, mTLE with Ammon's horn sclerosis is associated with pyramidal cell loss in predominantly in the CA1 and CA4, whereas cells in the CA2 and the dentate gyrus are generally more preserved.[85] Therefore, targeting may need to be individualized (e.g., via MRI-guided CED) to some extent depending on the particular patient pathology in order to prioritize more preserved hippocampal regions.

There was an increase in NPY abundance in the CSF, but not blood plasma, of AAV9.NPY-Y2R-receiving baboons, specifically, pre- and post-dosing in the same animals (Figures S8A and S8B). However, NPY levels in plasma and CSF of SPK100.NPY-Y2R-treated animals remained unchanged pre- and post-dosing, with plasma NPY levels remaining nearly undetectable 1 month after delivery, suggesting minimal peripheral exposure to vector or transgene protein after intraparenchymal administration of SPK100.NPY-Y2R. While these results may reflect differences in AAV9 versus AAV-Spark100 capsid transduction and biodistribution in the baboon, conclusions are limited by the small number of animals in this study as well as the exploratory nature of our novel, surgical approach. This initial study aimed to pilot/optimize intrahippocampal delivery of AAV in baboons and provides encouraging data for leveraging this model in future, direct-injection routes of AAV administration to the brain. These findings indicate that AAV.NPY-Y2R delivery to the baboon hippocampus was well tolerated and effective, and that the AAV-Spark100 capsid confers comparable transduction of hippocampal tissue to AAV9 in this model.

Overall, our results demonstrate the feasibility of safely and accurately delivering SPK100.NPY-Y2R into the hippocampus of an NHP, with favorable biodistribution and minimal spread beyond the temporal lobe. In the baboon study, we tested a single dose of the novel SPK100.NPY-Y2R vector to assess its feasibility, tolerability, and biodistribution following intraparenchymal delivery to the hippocampus. Moving forward, this work will guide the establishment of an efficacious dose range of this new vector (including the minimal effective dose) and a thorough evaluation of its safety, tolerability, and biodistribution before proceeding to human trials. It will also be important to expand upon the SPK100.NPY-Y2R rodent efficacy findings reported here and evaluate the minimal effective dose in a model presenting with spontaneous recurrent seizures, such as the kainic acid-induced mouse model of post-status epilepticus seizures.[86] Additionally, given the intraparenchymal delivery approach, it will be important to optimize hippocampal coverage while avoiding off-target leakage. The differences in weight gain observed with NPY-Y2R overexpression between rodents and baboons highlight the need to model potential on- and off-target effects in the appropriate species, using the same doses and surgical delivery methods proposed for human use.

In conclusion, our findings lend support toward the use of baboons as a model system for evaluating biodistribution of AAV-based gene therapies following intraparenchymal delivery. These results provide a solid foundation for advancing the safe and effective delivery of an AAV-based gene therapy overexpressing NPY and Y2R in the hippocampus for treating seizures in patients with TLE.

MATERIALS AND METHODS

Vector design and production

SPK100.NPY-Y2R is a single-stranded, (rAAV vector consisting of a bioengineered capsid (AAV-Spark100) and an expression cassette containing the human NPY coding sequence and human Y2R coding sequence separated by an IRES and downstream of a ubiquitously active, cytomegalovirus immediate-early enhancer/β-actin (CAG) promoter. The vector also contains a modified WPRE and the BGHpA, as previously described.[26] The same construct was encapsulated in the AAV9 serotype to generate AAV9.NPY-Y2R. For comparison of AAV1, AAV9, and AAV-Spark100 serotypes in mice (Figures S3 and S4), the same expression cassette above was modified

Table 2. Calcium imaging methods

Endpoint	Description
Active object count (total active neurons)	the number of objects that burst at least once above the minimum burst threshold over the total scan time
Mean intensity (mean calcium signal intensity)	the mean fluorescence intensity of an object over the total scan time. All objects within the image are calculated individually and then values are averaged
Mean burst rate (per min)	the number of calcium bursts over the total scan time divided by the scan time in minutes
Mean burst strength (mean calcium signal intensity area)	the area under each calcium burst divided by the duration of that burst is calculated individually and then values are averaged

Calcium imaging parameters measured using Incucyte Neuronal Activity Analysis Software Module for *in vitro* experiments in primary cortical neurons.

to contain only the human NPY coding sequence with the same CAG promoter, modified WPRE, and BGHpA retained.

All vectors were manufactured by transient, triple transfection of HEK293 cells in adherent culture, purified from clarified cell lysates by density gradient centrifugation, and then diafiltrated into an isotonic formulation. Titer was determined by means of quantitative polymerase chain reaction (qPCR).

Culturing of rat cortical neurons

Primary rat cortical neurons (Sprague Dawley, Thermo Fisher Scientific, cat. no. A36512) were seeded (35,000 cells per well) onto poly-D-lysine-coated 96-well optical plates (PerkinElmer PhenoPlate, cat. no. 6055300) in neuronal plating medium (Neurobasal Plus medium [Thermo Fisher Scientific, cat. no. A3582901], B-27 Plus Supplement [Thermo Fisher Scientific, cat. no. A3582801], GlutaMAX Supplement [Thermo Fisher Scientific, cat. no. 350500061], and fetal bovine serum [10%]) and cultured at 37°C, 5% CO_2. Half-medium changes were performed the day after plating and three times per week using neuronal medium (Neurobasal Plus medium, B-27 Plus Supplement, GlutaMAX Supplement, and penicillin/streptomycin [0.5%]).

Calcium imaging

Primary rat cortical neurons were transduced with the Incucyte NeuroBurst Orange Lentivirus (Sartorius, cat. no. 4736) reagent delivering a proprietary, genetically encoded calcium indicator (mRuby based) driven by a synapsin promoter on day *in vitro* 4 (DIV4). Neurons were incubated in the Incucyte SX5 Live-Cell Analysis System (37°C, 5% CO_2) for long-term, calcium imaging. Two, 75% medium changes with neuronal medium (see above) were performed the day after lentiviral infection (DIV5) to avoid oxygen exposure to the neurons.

Neurons were transduced with AAV (5×10^5 viral genomes per cell or 5×10^6 viral genomes per cell) diluted in neuronal medium on DIV7. Two, 75% media changes with neuronal medium were performed the day after AAV infection (DIV8). Calcium signals (minimum burst threshold was defined as 0.2 relative fluorescence units) were recorded in the Incucyte system twice daily until DIV35. Using the Incucyte Neuronal Activity Analysis Software Module (Sartorius, *cat.* no. 9600-0032), the parameters outlined in Table 2 were measured and averaged per well per day.

Immunocytochemistry

Brain cortices were harvested from embryonic day 18 (E18) rat embryos (Sprague-Dawley, Janvier Labs, Le Genest-Saint-Isle, France), and dissociated enzymatically and mechanically. Dissociated cells (10,000 cells per well) were plated in poly-D-lysine-coated imaging plates (384-well) (Corning, cat. no. 356663) in neuronal growth medium (Neurocult Neuronal Basal medium [Fisher Scientific, cat. no. 11570556], SM1 neuronal supplements, L-glutamine, and HEPES). Cells were incubated at 37°C, 5% CO_2, with half-medium changes occurring every 3–4 days. Cells were infected with AAV on day 3 *in vitro*, and immunocytochemistry initiated on day 14 *in vitro*. Cells were infected with five different multiplicities of infection of AAV-Spark100.CAG-eGFP: 5×10^4, 1×10^5, 5×10^5, 1×10^6, or 5×10^6 viral genomes per cell.

Immunocytochemistry was performed to quantify the transduction efficiency of the AAV-Spark100 capsid using a reporter vector (AAV-Spark100.CAG-eGFP). Briefly, wells were rinsed with cold phosphate-buffered saline (PBS) and then fixed in 4% paraformaldehyde solution for 20 min at room temperature (RT). Cells were permeabilized using 0.1% Triton for 10 min at RT then rinsed with PBS. Next, cells were incubated in a blocking solution (10% normal goat serum) for 30 min then rinsed with PBS. Primary antibodies were dissolved in PBS at the following dilutions and incubated overnight at 4°C: Chicken anti-MAP2 antibody (BioLegend, cat. no. 822501), 1 to 1,000. After two PBS washes, cells were incubated with secondary antibody for 1 h at RT: goat anti-chicken Alexa Fluor 647 (Invitrogen, cat. no. A21449), 1 to 500. After two PBS washes, cells were incubated with DAPI to stain nuclei (1 μg mL^{-1} final). Images were acquired using a fluorescence microscope platform (HSC ArrayScan VTI microscope, 20× images). The number of GFP-positive cells co-localized with MAP2 was evaluated and expressed as a percentage.

Animals

Mice

Male, naive mice (C57BL/6JRj; Janvier Labs) were used for all *ex vivo* MEA experiments, and were acclimated to the test facility for at least 5 days prior to study initiation. Mice were 8 weeks old and weighed

Table 3. Intrahippocampal infusion coordinates for mouse

Target	Anterior-posterior to bregma (mm)	Lateral to bregma (mm)	Ventral from skull surface at trajectory (mm)	Volume (μL)
Dorsal hippocampus 1	−2.0	±1.5	−2.0	1
Dorsal hippocampus 2	−2.0	±1.5	−2.4	1
Ventral hippocampus 1	−3.0	±3.0	−2.8	1.5
Ventral hippocampus 2	−3.0	±3.0	−4.3	1.5

Stereotactic coordinates and infusate volumes used for intrahippocampal delivery of AAV in mice. Note that the ventral coordinates are relative to the skull surface above the intended ventral trajectory and not relative to bregma or dura.

approximately 25–35 g at the beginning of the experiment. Mice were group-housed in macrolon cages (no more than 10 animals per cage) on wood litter (SAFE, 89290 Augy, France). Environmental enrichment (e.g., tunnel, gnawing material, nesting material, etc.) was provided. Mice were housed under controlled temperature (22°C ± 2°C) conditions with a 12-h light/dark cycle. Food and water were provided *ad libitum*. Terminal body weight was collected for all animals at the study endpoint.

Synapsin TKO mice on the C57BL/6 N genetic background were kindly provided by Dr. Flavia Valtorta at the Vita-Salute San Raffaele University (Milan, Italy), and have previously been described.[87] Male, TKO mice were housed under controlled temperature (22°C ± 1°C) and humidity (50%) conditions with a 12-h light/dark cycle. Food and water were provided *ad libitum*. The weight of the animals was monitored weekly, beginning on the first day of surgery at postnatal day 45, until the study endpoint.

Rats

Young adult, male Sprague-Dawley rats (225–250 g) from Taconic Biosciences (Germantown, NY) were used for electrical kindling experiments and group housed in ventilated cages in groups of 2–3 per cage. All rats were acclimated to the colony room for at least 1 week before testing. After surgical implantation of EEG stimulating/recording electrodes, each animal was single housed for the remainder of the study with enrichment. Rats were examined on a regular basis, handled, and weighed to assure adequate health and suitability. Rats were housed under controlled temperature (20°C–23°C) and humidity (50%) conditions with a 12-h light/dark cycle. Food and water were provided *ad libitum* for the duration of the study.

Intracranial delivery of adeno-associated viral vectors

Mice

Mice (C57BL/6JRj [Janvier Labs] or TKO mice described above) were anesthetized under isoflurane anesthesia (5% for induction and 2% for maintenance, under 100% O_2) and placed in a stereotaxic frame. Animals were given 5 mg kg^{-1} carprofen (Rimadyl) subcutaneous (s.c.) on the back. A midline sagittal incision was made in the scalp and holes were drilled in the skull bilaterally using the coordinates outlined in Table 3.

For *ex vivo* MEA experiments, each mouse received bilateral injections of either vehicle (vector diluent) or AAV-Spark100.NPY-Y2R (6×10^{11}, 1.9×10^{12}, or 6×10^{12} vg mL^{-1}) into the dorsal and ventral hippocampus (6×10^{9}, 1.9×10^{10}, or 6×10^{10} vg total per animal). For experiments in TKO mice, animals received bilateral injections of either vehicle (vector diluent) or AAV9.NPY-Y2R (1×10^{13} vg mL^{-1}; 5×10^{10} vg total per animal) into the dorsal and ventral hippocampus. Infusions were performed at 0.4 μL min^{-1} through a 33-gauge (G) stainless steel needle (beveled needle point [point style 4]) using a 5 μL Hamilton Neuros 700 Series syringe (Hamilton, cat. no. 14-785-709) mounted on a vertical perfusor (Harvard apparatus, cat. no. 70–4507). Delivery coordinates and infusion volumes are outlined in Table 3. At each trajectory, the more dorsal coordinate was infused first prior to moving down to the more ventral coordinate. After each infusion, the cannula was left in place for 5 min to prevent backflow of the infusate along the cannula track. At the end of surgery, the animals were placed on a heat pad until awakening. The animals were given 5 mg kg^{-1} carprofen (Rimadyl) s.c. at 24- and 48-h post-surgery.

Rats

Rats (young adult, male Sprague-Dawley rats [225–250 g] from Taconic Biosciences) underwent two separate, stereotactic surgeries for intraparenchymal injections and electrode implantation (see EEG electrode implantation and recordings below), respectively. Rats received Meloxicam-SR s.c. in the interscapular region (4.0 mg kg^{-1}) immediately prior to each surgery, and were anesthetized under isoflurane anesthesia (3% for induction and 2% for maintenance, under 100% O_2). The scalp was prepared for surgery by cleaning the clipped injection site with Povidone iodine and a 70% ethanol rinse. A 1.5–2 cm center incision was made in the scalp.

Animals received bilateral, intraparenchymal injections of either vehicle (vector diluent) or AAV-Spark100.NPY-Y2R into the hippocampus. Two 33-G stainless steel [blunt needle point (point style 3)] injector cannulas (Plastics One, C315I) were used for simultaneous bilateral injections with a glass Hamilton syringe. Each stainless steel injector cannula was attached to a 50 μL glass Hamilton syringe (Hamilton, cat. no. 1705) via polyethylene (PE-50) tubing (Plastics One, cat. no. C232C). The injection needle/cannula was attached to a stereotaxic apparatus (Model 942, David Kopf Instrument), and the Hamilton syringes were operated by an injection pump (Stoelting Dual Syringe Pump, Model 210). Rats was infused with either 1.3 or 1.13 μL of dosing solution (1×10^{12} or 1×10^{13} vg mL^{-1}) into each injection site, bilaterally (total 10 injections, 5 per

Table 4. Intrahippocampal infusion coordinates for rat

Target	Anterior-posterior to bregma (mm)	Lateral to bregma (mm)	Ventral from skull surface at trajectory (mm)	Volume (μL)
Dorsal hippocampus 1	−3.7	±2.2	−2.8	1.3
Dorsal hippocampus 2	−3.7	±2.2	−3.7	1.3
Ventral hippocampus 1	−5.8	±5.1	−4.0	1.13
Ventral hippocampus 2	−5.8	±5.1	−5.6	1.13
Ventral hippocampus 3	−5.8	±5.1	−7.3	1.13

Stereotactic coordinates and infusate volumes used for intrahippocampal delivery of AAV in rats. Note that the ventral coordinates are relative to the skull surface above the intended ventral trajectory and not relative to bregma or dura.

hemisphere) at a rate of 0.5 μL min^{-1} and with a 5 min rest period following each injection (1.2×10^{10} or 1.2×10^{11} vg total per animal). See Table 4 for coordinates and infusion volumes at each target trajectory. At each trajectory, the more ventral coordinate was infused first prior to moving up to the more dorsal coordinate.

Ex vivo MEA recordings

Acute hippocampal slices were obtained from either naive (NPY peptide experiments) or AAV-injected (3 weeks prior; SPK100.NPY-Y2R experiments), adult male mice (C57BL/6JRj; Janvier Labs). Briefly, mice were sacrificed by decapitation, and their brains immediately removed and placed in chilled (4°C) artificial CSF (aCSF) oxygenated with a carbogen gas mixture (95% O_2; 5% CO_2). Composition of aCSF was as follows: 124 mM NaCl, 3.5 mM KCl, 1.5 mM $MgSO_4$, 1.2 mM NaH_2PO_4, 2.5 mM $CaCl_2$, 26 mM $NaHCO_3$, 12 mM D-glucose. Transverse hippocampal slices (400 μm thick) were cut using a tissue slicer (Stoelting tissue slicer, cat. no. 51425) and maintained for 1 h in warmed and oxygenated aCSF (28°C).

After a minimum of 1 h of recovery at 28°C, hippocampal slices were placed in a MEA well (Multi Channel System, Germany, MEA2100, 60 electrodes; electrode spacing: 100 μm) for *ex vivo* recordings and maintained with a harp slice grid. To evaluate the health of each slice, an electrical pulse (internal MEA electrode, 100 μs, 3,000–5,000 mV) was delivered to the Schaffer collaterals of the hippocampal formation. Dendritic responses were obtained in the CA1 area. The stimulation and recording electrodes were chosen according to the placement of the slice in the MEA well. Slice placement was monitored via a camera placed under the MEA well to maintain the same distance between stimulation electrode and recording electrode for each slice. Hippocampal slices with acceptable CA1 responses to Schaffer collateral stimulation were subsequently used for the experimental recordings (fEPSP amplitude between −500 mV s^{-1} and −1,000 mV s^{-1} with good shape obtained following electrical stimulation of Schaeffer collaterals at 3,500 mV). Both ventral and dorsal hippocampal slices were tested in the NPY peptide experiment, and only dorsal hippocampal slices were tested in the SPK100.NPY-Y2R experiments.

Spike detection threshold was set such as the amplitude of the signal was seven times higher than the baseline (background). This was automatically adjusted by the software for each electrode and each slice. Burst detection parameters were as follows: maximum (max) interval to start burst, 10 ms; max interval to end burst, 50 ms; minimum (min) interval between bursts, 100 ms; min duration of burst, 200 ms; min number of spikes in burst, 6.

NPY peptide experiments

After 10 min of baseline recording, the respective treatment (0.1 μM NPY, 0.5 μM NPY, 1 μM NPY, or 1 μM NPY with 0.6 μM BIIE0246) or reference substance (Retigabine, 10 μM) was bath applied for 20 min before adding 4-AP (∼2.65 mL min^{-1}). After the addition of 100 μM 4-AP (a voltage-gated potassium channel blocker), recordings were performed for an additional 20 min for a total of 50 min of recordings. See schematic of experimental timeline for NPY peptide experiments in Figure S10. Experiments included a total of $n = 8$ hippocampal slices per group (1–3 slices per mouse from 3 to 5 naive mice).

The following parameters were assessed in the CA1 and CA3 region of each hippocampal slice: change in mean number of spikes over the treatment period (20–30 min) or over 4-AP period (40–50 min) from baseline (0–10 min) and change in mean number of bursts over the treatment period (20–30 min) or over 4-AP period (40–50 min) from baseline (0–10 min).

SPK100.NPY-Y2R experiments

Slice harvesting and recording took place 3 weeks after intrahippocampal SPK100.NPY-Y2R delivery. A 10 min baseline recording was first performed for all slices. The reference substance (Retigabine, 10 μM) was then bath applied 20 min prior to 4-AP perfusion (∼2.65 mL min^{-1}) for slices receiving Retigabine. After baseline recordings, all slices had 100 μM 4-AP bath applied, and then were recorded for an additional 20 min for a total of 50 min of recordings. See schematic of experimental timeline for vector experiments in Figure S11. Experiments included a total of $n = 10$ dorsal hippocampal slices per group (1 slice per mouse from 10 SPK100.NPY-Y2R-treated mice).

The following parameters were assessed in the CA1 and CA3 region of each hippocampal slice: mean number of spikes and bursts prior to 4-AP addition (20–30 min); mean number of spikes and bursts over the 4-AP period (40–50 min).

EEG electrode implantation and recordings

Mice

TKO mice intended for video-EEG recordings underwent surgery for a transmitter implant between age 52 and 55 days, and 1 week after the delivery of vehicle or AAV. The ETA-F10 transmitter (Data Sciences International, St. Paul, MN) was positioned in a subcutaneous pocket on the back of the mouse with the wires guided to the skull. The recording electrode was placed on the dura mater above the hippocampus, and the reference electrodes were placed contralaterally on the dura mater, anterior to the bregma. Once the electrodes were in position, dental cement (Harvard Apparatus) was added to cover and attach the implant to the skull.

Video-EEG recording started 2 weeks after vehicle/AAV delivery and was performed continuously for 24 h a day, 7 days a week, over a period of 2 weeks. Neuroscore (Data Sciences International) was used for EEG analysis. All traces were visually inspected for the detection of seizures and duration was measured as the period of paroxysmal activity of high frequency (>5 Hz) characterized by a 3-fold higher amplitude over baseline with a minimum duration of at least 5 s.

Rats

Two to 3 weeks after intraparenchymal injections, rats underwent electrodes implantation for EEG recordings. A stimulating/recording electrode (two twisted, stainless steel wires, E363/3-2TW/SPC ELEC .005/.125MM SS 2TW, P1 Technologies) was placed into the ventral hippocampus for kindling and local field potential (LFP) recordings (unilaterally on right side of the brain: −4.8 mm caudal to bregma, +4.8 mm lateral to bregma, and −7.0 mm below the brain parenchyma surface). A stainless steel screw connected with a wire for EEG recordings was also implanted at the coordinates of +2 mm rostral to bregma, +3 mm lateral. A ground electrode was implanted −2 mm caudal to lambda (at the midline) and attached to a stainless steel screw. The entire electrode assembly was connected to a head stage attached to the skull with dental cement. EEG and LFPs were recorded during kindling. Data were acquired using the CED Data Acquisition and Analysis System (Cambridge Electronic Design), with Spike2 software for digitizing signals.

In vivo electrical kindling

Rapid kindling occurred at least 4 weeks following injection with vehicle or SPK100.NPY-Y2R. Before starting the data acquisition, the EEG signals were briefly inspected for their quality to eliminate any noise (60 Hz) or movement artifact. The animal was tethered to a stimulation/recording panel through a cable connected to its head mount. The depth electrode implanted into the right hippocampus was used as both the stimulation and recording electrode (field potential recording).

The stimulation threshold for each animal was determined prior to the rapid kindling session. Stimulating intensity started at 10 μA (1 ms monophasic square wave pulses, 100 Hz, 1 s duration) and was subsequently increased by 10 μA steps until a maximum of 400 μA, or the animal displayed at least 5 s of afterdischarge via the LFP signal in the hippocampal, bipolar depth electrode. This intensity was defined and recorded as the afterdischarge threshold. Surface EEG was recorded simultaneously through the screw electrode to reveal the spread of the afterdischarge signal.

The procedure for rapid kindling started immediately after the threshold testing. During the rapid hippocampal kindling procedure, animals were stimulated with 40, suprathreshold stimulations (400 μA) of a monophasic square wave current (1 ms square wave pulses, 10 Hz, 10 s duration) with an inter-stimulation interval of 5 min. Focal epileptiform activity (afterdischarge duration) was detected via the LFP signal in the hippocampal, bipolar depth electrode and screw electrode after each stimulation episode. All behavioral seizure scoring was performed by a researcher blinded to treatment group. The following endpoints were measured for each rat tested: (1) threshold current (the current intensity [μA] at which an animal displayed at least 5 s of afterdischarge via the EEG signal measured from the hippocampal depth electrode prior to undergoing kindling), (2) afterdischarge duration (afterdischarge duration [s] following each, 400 μA stimulation episode of the rapid kindling test from both the hippocampal depth electrode and the EEG surface electrodes), (3) seizure severity (behavioral seizure score [Racine scale] after each, 400 μA stimulation episode of the rapid kindling test), and (4) number of seizure events (the total number of events at each Racine seizure stage observed).

All rats were euthanized 2 weeks after the rapid kindling paradigm and had each hippocampus individually micro-dissected for downstream bioanalysis of vector genome copies and NPY protein abundance.

MRI-guided CED of AAV9 and AAV-Spark100 to baboon hippocampus

Six female, adult baboons (*Papio hamadryas*; 9.0–12.0 kg) were included in this biodistribution study. Animals were screened for the presence of antibodies to AAV9 and SPK100 capsids prior to dosing and were considered seronegative with serum neutralizing antibody titers lower than 1:1 at baseline. Serum samples for each animal were collected and analyzed for neutralization capacity against the capsids being used (AAV-Spark100 and AAV9) in a cell-based transduction assay using values derived from reciprocal dilution to determine a dilution in which relative luminescence units were reduced by 50% compared with control wells. Animals selected for this study had low or no detectable NAbs for the capsid being used.

For intraparenchymal infusion of AAV9/SPK100.NPY-Y2R, animals were sedated with ketamine (8 mg kg^{-1}) and dexmedetomidine (0.02 mg kg^{-1}) and then maintained under anesthesia with isoflurane. All animals were treated with levetiracetam (10 mg kg^{-1}) prophylactically to prevent seizure activity. Then, animals were placed prone in an MRI-compatible ClearPoint Pre-Clinical Orchestra Frame and underwent MRI-guided CED using the ClearPoint SmartFlow MR Compatible Ventricular Cannula (cat. no. CUS-SMFL-03) to deliver

approximately 200 μL (1×10^{11} vg mL^{-1}) of an AAV9.NPY-Y2R or SPK100.NPY-Y2R dosing formulation containing 2 mmol L^{-1} contrast agent (ProHance) into the right hippocampus. All baboons also received approximately 200 μL (1×10^{11} vg mL^{-1}) of an AAV9 or AAV-Spark100 reporter vector (AAV9/SPK100.CAG-dTomato) dosing formulation into the contralateral (left) hippocampus containing 2 mmol L^{-1} contrast agent (ProHance). MRI sequences, ClearPoint hardware, and ClearPoint software were used to plan trajectories and enable cannula placement at the identified infusion target locations within the hippocampus. Upon completion of the first infusion, MRI contrast on post-infusion scans was analyzed for distribution of hyperintense signal.

Veterinary personnel monitored all animals after AAV delivery until the end of the study to identify any possible adverse effects. Cage-side observations were also performed twice daily throughout the study to evaluate general health, appearance, and appetite in all animals. Cage-side neurological assessment for signs of neurological impairment, specifically, were performed at baseline and then 2, 7, 14, and 29 days post-surgery. Animals were weighed prior to surgery, and then again 2, 7, and 30 (terminal) days after surgery. None of the animals showed any adverse effects.

Blood plasma and CSF were collected from each animal for analysis of NPY protein abundance by ELISA. Blood plasma was collected at baseline, 2 days post-surgery, 7 days post-surgery, and the day of necropsy (30 days post-surgery). CSF was collected at baseline and the day of necropsy (30 days post-surgery). Animals were fasted and anesthetized with ketamine and dexmedetomidine for all scheduled blood and CSF sample collection procedures. Blood was collected by femoral, cephalic, or saphenous venipuncture; CSF was collected by lumbar puncture procedure.

After surgery (30 ± 3 days), all animals were anesthetized with ketamine and dexmedetomidine to obtain terminal body weight, blood, and CSF samples. Following blood and CSF samples collection, animals were transitioned to isoflurane anesthesia and underwent transcardial perfusion with cold 1× PBS (Fisher Scientific, cat. no. BP24384) to exsanguinate them from the right atrium. Alternating, 4 mm coronal slabs of the brain were collected for either formalin-fixation and subsequent histology or fresh tissue biopsies (2–4 mm punches) for bioanalysis of vector genome copies and NPY protein abundance. Coronal brain slabs (4mm) for histology were submerged in 10% neutral-buffered formalin for 48 h and then transferred to 70% ethanol prior to paraffin-embedding. Fresh frozen tissue biopsies were immediately flash frozen.

Bioanalysis of vector biodistribution and transgene expression

Co-extraction of DNA and protein

Micro-dissected brain tissues were homogenized in N-PER Neuronal Protein Extraction Reagent (Thermo Fisher Scientific, cat. no. 87792) containing Halt Protease and Phosphatase Inhibitor Cocktail, 100× (Thermo Fisher Scientific, cat. no. 78440) with one stainless steel bead (QIAGEN, cat. no. 69989) using a TissueLyser (QIAGEN) at 25 Hz for 20 s, twice. A portion of the homogenized sample (two-thirds) was transferred to a new tube and reserved for DNA extraction. Homogenized samples for protein extraction were incubated on a rotator for 20 min at 4°C, centrifuged at 21,000 × *g* for 20 min at 4°C to pellet the cell debris, and had the resultant supernatant collected as total protein extract. Total protein was quantified using a Pierce BCA Protein Assay Kit (Thermo Fisher Scientific, cat. no. 23225). DNA was extracted using a DNeasy Blood & Tissue Kit (QIAGEN, cat. no. 69506), and DNA concentrations were determined using a NanoDrop.

Vector biodistribution

Vector genome levels were assessed by a real-time qPCR assay multiplexed to detect 2 targets: CAG.NPY-Y2R vector DNA and mouse/rat/baboon glyceraldehyde 3-phosphate dehydrogenase DNA. Standard curves were generated by serially diluting 1:10 a stock solution containing linearized ss.CAG.NPY-Y2R plasmid, mouse/rat/baboon gDNA, and Salmon Sperm DNA (Agilent, cat. no. PN201190). qPCR was run with the TaqMan Multiplex Master Mix (Thermo Fisher Scientific, cat. no. 4461881) on a QuantStudio Flex7 system, using custom primer/probe sets from Integrated DNA Technologies. Standard curves were analyzed to ensure a qPCR efficiency of 100 ± 10% (slope between −3.6 and −3.3) and $R^2 > 0.98$. Vector genome copies were reported as vector copies per μg DNA.

NPY protein expression analysis

NPY protein levels from tissue samples were analyzed using Simple Western Automated Western Blot Systems (Protein Simple) with the 2–40 kDa Separation Module for WES or Sally Sue (Protein Simple, cat. no. SM-W009 and cat. no. SM-S003) according to the manufacturer's instruction. NPY protein was detected with rabbit anti-Neuropeptide Y (D7Y5A) XP (Cell Signaling Technology, cat. no. 11976) at a 1 to 25 dilution. Cofilin protein was assessed as a loading control using rabbit anti-Cofilin (Novus Biologics, cat. no. NB100-1900) at a 1 to 200 dilution. The anti-rabbit detection module (Protein Simple, cat. no. DM-001) was used according to the manufacturer's instruction. Recombinant NPY protein (Sigma, cat. no. *N5017*) was used to generate a standard curve by serial 2-fold dilutions from 150 to 1.95 ng mL^{-1}. NPY protein levels in samples were extrapolated from the standard curve and back-calculated to account for the dilution factor, and reported as ng mL^{-1} of total protein (normalized to Cofilin).

NPY protein levels from *Papio hamadryas* (baboon) blood plasma and cerebrospinal fluid were analyzed by ELISA (Human NPY ELISA, Sigma, cat. no. EZHNPY-25K) according to the manufacturer's instructions. NPY protein levels in samples were extrapolated from the kit standard curve and reported as pg mL^{-1} of total sample.

Immunohistochemistry of NPY and Y2R proteins

Formalin-fixed brain samples from mice and baboons were paraffin-embedded using an automated tissue processor (Sakura Finetek USA, model Tissue-Tek VIP 6 AI, SN 60400848-0221). Paraffin blocks were cut into 5 μm thick sections using a microtome

(Leica, model RM2255, SN 13102). Immunofluorescence staining for NPY was performed with an automated instrument (Leica, model Bond RX, cat. no. 3498291) using rabbit anti-Neuropeptide Y (Abcam, cat. no. ab30914) at a 1 to 2000 dilution for 6 h at RT followed by donkey anti-rabbit Alexa Fluor 647 (Jackson ImmunoResearch, cat. no. 711-605-152) secondary antibody at a 1 to 1,000 dilution for 1 h at RT. Slides were counterstained with DAPI, coverslipped, and imaged with a 20× objective lens using a slide scanner (Axio Scan Z1, Zeiss).

For experiments in TKO mice, brains were fixed in 4% paraformaldehyde for 16 h at 4°C before being cryoprotected in 30% sucrose in 1× PBS for 2 days. Brains were then embedded in Killik, O.C.T. (Bio-Optica), rapidly frozen, and cut into 50 μm thick coronal sections using a CM3050s cryostat (Leica Microsystems). Free-floating slices were incubated with a blocking solution containing 1% normal goat serum and 0.3% Triton in 1× PBS for 1 h at RT. The immunofluorescence procedure for Y2R also included heat-induced antigen retrieval with sodium citrate (10 mM sodium citrate [pH 6.0]) at 75°C for 20 min. Immunofluorescence staining for NPY and Y2R was performed using rabbit anti-Neuropeptide Y (Cell Signaling Technologies, cat. no. 11975) at a 1 to 250 dilution or rabbit anti-NPY2R (Neuromics, cat. no. RA14112) at a 1 to 200 dilution overnight at 4°C followed by goat anti-rabbit Alexa Fluor 488 (Thermo Fisher, cat. no. A-11008) secondary antibody at a 1 to 1,000 dilution for 1.5 h at RT. Slices were counterstained with DAPI (5 mg mL^{-1}; 5 min) and then mounted onto microscope slides. Once dried (at 50°C), coverslips were mounted with DAKO fluorescent mounting medium (Agilent), and images were acquired with a Mavig RS-G4 Confocal. Image analysis and composition were performed with Fiji ImageJ software.

Statistics

For *in vitro* experiments, we chose similar sample sizes for Ca^{2+} imaging readouts in primary neuronal cultures based on published literature and pilot studies performed in-house. Each endpoint was analyzed using a mixed effects model, where "treatment" and "time" were modeled as fixed effects and "well" was modeled as a random effect, followed by a Šídák's or Holm- Šídák's multiple comparisons test.

The number of animals/slices used in *ex vivo* and *in vivo* experiments was predetermined prior to the start of each experiment based on pilot studies to establish innate model variability as well as predicted effect size. All datasets were analyzed using the Shapiro-Wilk test for normality. For 2-sample comparisons, datasets with normal distributions were analyzed for significance using the unpaired Student's t test, whereas datasets with nonnormal distributions were analyzed using the Mann-Whitney U test. For three-sample comparisons, datasets with normal distributions were analyzed for significance using a standard, one-way analysis of variance (ANOVA) with a post hoc Holm-Šídák's multiple comparisons test, whereas datasets with nonnormal distributions were analyzed using the Kruskal-Wallis test with a post hoc Dunn's multiple comparisons test. One- or two-way, repeated measures ANOVA was conducted for the appropriate datasets with a post hoc Dunnett's or Dunn's multiple comparisons tests. All comparisons were two-tailed.

All graphs are plotted using Prism (GraphPad). Bolded center lines reflect the mean, and all error bars indicate standard deviation.

Study approvals

Animal experiments were conducted in accordance with the ethical guidelines of the NIH and with the approval of the Institutional Animal Care and Use Committee of PsychoGenics (rat studies) or ClearPoint, Neuro (baboon study), or the Animal Health regulations of France and in accordance with the Association for Assessment and Accreditation of Laboratory Animal Care (AAALAC) and Porsolt's Ethical Committee (mouse studies). TKO mice were maintained and bred at the animal house of Ospedale San Raffaele in compliance with institutional guidelines and international laws (EU Directive 2010/63/EU EEC Council Directive 86/609, OJL 358, 1, December 12, 1987, NIH Guide for the Care and Use of Laboratory Animals, U.S. National Research Council, 1996). All efforts were made to minimize animal suffering.

DATA AVAILABILITY

Information for all viral vectors and antibodies used is provided in the materials and methods section. All other relevant data are available from the authors upon request.

ACKNOWLEDGMENTS

This work was funded by Spark Therapeutics. The authors would like to thank the following team members at Spark for their contributions: the Histology Team (Renee Genztel, Ashley Carter, Kelly Quednau-Ekanger, Mohamad Nayal, and Timothy Baradet) for histology of baboon brains, the Preclinical Bioanalytics Team (Heena Beck, Mani Kandasamy, and Tieng Pham) for analysis of NPY protein from baboon CSF and plasma samples, Jodi McBride for valuable experimental expertise and guidance during baboon surgical planning, and Benjamin Okyere and Juliet Mengaziol for their assistance in protein analysis from *ex vivo* MEA experiments. The authors would also like to thank the teams at Porsolt (Le Genest-Saint-Isle, France) for *ex vivo* MEA experiments, PsychoGenics, Inc. (Paramus, NJ) for rat rapid kindling experiments, and ClearPoint Neuro, Inc. (San Diego, CA) for intraparenchymal infusion of vector to baboons. Figures were created with BioRender.com.

AUTHOR CONTRIBUTIONS

B.T., E.M., P.F., D.D., and L.M. designed the experiments and reviewed and interpreted the data. B.T., D.D., S.C., and I.G. performed the experiments with assistance from additional team members at Spark Therapeutics. K.A., E.R., B.B., M.S., and M.K. provided valuable experimental feedback and guidance. B.T. wrote the manuscript with input from all other authors. All authors approved the final version before submission.

DECLARATION OF INTERESTS

This work was funded by Spark Therapeutics, Inc. B.T., D.D., L.M., and E.R. are employees of Spark Therapeutics, Inc. E.M. and P.F. are employees of CombiGene AB. K.A. is a former employee of CombiGene AB, and a current employee of Epigenica. M.K. is co-founder of CombiGene AB, and E.M. and M.K. own stock in CombiGene AB. L.M. has an unpaid visiting academic affiliation at King's College, University of London. This work is related to patent registrations WO 2017/137585 and WO 2008/004972.

SUPPLEMENTAL INFORMATION

Supplemental information can be found online at https://doi.org/10.1016/j.ymthe.2025.06.019.

REFERENCES

1. Manole, A.M., Sirbu, C.A., Mititelu, M.R., Vasiliu, O., Lorusso, L., Sirbu, O.M., and Ionita Radu, F. (2023). State of the Art and Challenges in Epilepsy—A Narrative Review. J. Pers. Med. *13*, 623. https://doi.org/10.3390/jpm13040623.
2. Engel, J. (1996). Introduction to temporal lobe epilepsy. Epilepsy Res. *26*, 141–150. https://doi.org/10.1016/s0920-1211(96)00043-5.
3. Téllez-Zenteno, J.F., and Hernández-Ronquillo, L. (2012). A Review of the Epidemiology of Temporal Lobe Epilepsy. Epilepsy Res. Treat. *2012*, 1–5. https://doi.org/10.1155/2012/630853.
4. Kuzmanovski, I., Cvetkovska, E., Babunovska, M., Kiteva Trencevska, G., Kuzmanovska, B., Boshkovski, B., and Isjanovska, R. (2016). Seizure outcome following medical treatment of mesial temporal lobe epilepsy: Clinical phenotypes and prognostic factors. Clin. Neurol. Neurosurg. *144*, 91–95. https://doi.org/10.1016/j.clineuro.2016.03.018.
5. Alessio, A., Damasceno, B.P., Camargo, C.H.P., Kobayashi, E., Guerreiro, C.A.M., and Cendes, F. (2004). Differences in memory performance and other clinical characteristics in patients with mesial temporal lobe epilepsy with and without hippocampal atrophy. Epilepsy Behav. *5*, 22–27. https://doi.org/10.1016/j.yebeh.2003.10.010.
6. Steiger, B.K., Muller, A.M., Spirig, E., Toller, G., and Jokeit, H. (2017). Mesial temporal lobe epilepsy diminishes functional connectivity during emotion perception. Epilepsy Res. *134*, 33–40. https://doi.org/10.1016/j.eplepsyres.2017.05.004.
7. (2004). Mesial Temporal Lobe Epilepsy with Hippocampal Sclerosis. Epilepsia *45*, 695–714. https://doi.org/10.1111/j.0013-9580.2004.09004.x.
8. Asadi-Pooya, A.A., Stewart, G.R., Abrams, D.J., and Sharan, A. (2017). Prevalence and Incidence of Drug-Resistant Mesial Temporal Lobe Epilepsy in the United States. World Neurosurg. *99*, 662–666. https://doi.org/10.1016/j.wneu.2016.12.074.
9. Qian, J., Colmers, W.F., and Saggau, P. (1997). Inhibition of Synaptic Transmission by Neuropeptide Y in Rat Hippocampal Area CA1: Modulation of Presynaptic Ca2+ Entry. J. Neurosci. *17*, 8169–8177.
10. Sorensen, A.T., Kanter-Schlifke, I., Lin, E.J., During, M.J., and Kokaia, M. (2008). Activity-dependent volume transmission by transgene NPY attenuates glutamate release and LTP in the subiculum. Mol. Cell Neurosci *39*, 229–237. https://doi.org/10.1016/j.mcn.2008.06.014.
11. Powell, K.L., Fitzgerald, X., Shallue, C., Jovanovska, V., Klugmann, M., Von Jonquieres, G., O'Brien, T.J., and Morris, M.J. (2018). Gene therapy mediated seizure suppression in Genetic Generalised Epilepsy: Neuropeptide Y overexpression in a rat model. Neurobiol. Dis. *113*, 23–32. https://doi.org/10.1016/j.nbd.2018.01.016.
12. Foti, S., Haberman, R.P., Samulski, R.J., and McCown, T.J. (2007). Adeno-associated virus-mediated expression and constitutive secretion of NPY or NPY13-36 suppresses seizure activity in vivo. Gene Ther. *14*, 1534–1536. https://doi.org/10.1038/sj.gt.3303013.
13. Wickham, J., Ledri, M., Bengzon, J., Jespersen, B., Pinborg, L.H., Englund, E., Woldbye, D.P.D., Andersson, M., and Kokaia, M. (2019). Inhibition of epileptiform activity by neuropeptide Y in brain tissue from drug-resistant temporal lobe epilepsy patients. Sci. Rep. *9*, 19393. https://doi.org/10.1038/s41598-019-56062-1.
14. Erickson, J.C., Clegg, K.E., and Palmiter, R.D. (1996). Sensitivity to leptin and susceptibility to seizures of mice lacking neuropeptide Y. Nature *381*, 415–421.
15. Baraban, S.C., Hollopeter, G., Erickson, J.C., Schwartzkroin, P.A., and Palmiter, R.D. (1997). Knock-Out Mice Reveal a Critical Antiepileptic Role for Neuropeptide Y. J. Neurosci. *17*, 8927–8936.
16. Bannon, A.W., Seda, J., Carmouche, M., Francis, J.M., Norman, M.H., Karbon, B., and McCaleb, M.L. (2000). Behavioral characterization of neuropeptide Y knockout mice. Brain Res. *868*, 79–87. https://doi.org/10.1016/s0006-8993(00)02285-x.
17. Woldbye, D.P., Larsen, P.J., Mikkelsen, J.D., Klemp, K., Madsen, T.M., and Bolwig, T.G. (1997). Powerful inhibition of kainic acid seizures by neuropeptide Y via Y5-like receptors. Nat. Med. *3*, 761–764.
18. Ledri, M., Sørensen, A.T., Madsen, M.G., Christiansen, S.H., Ledri, L.N., Cifra, A., Bengzon, J., Lindberg, E., Pinborg, L.H., Jespersen, B., et al. (2015). Differential Effect of Neuropeptides on Excitatory Synaptic Transmission in Human Epileptic Hippocampus. J. Neurosci. *35*, 9622–9631. https://doi.org/10.1523/JNEUROSCI.3973-14.2015.
19. Pedragosa-Badia, X., Stichel, J., and Beck-Sickinger, A.G. (2013). Neuropeptide Y receptors: how to get subtype selectivity. Front. Endocrinol. *4*, 5. https://doi.org/10.3389/fendo.2013.00005.
20. Pickel, V.M., Chan, J., Veznedaroglu, E., and Milner, T.A. (1995). Neuropeptide Y and dynorphin-immunoreactive large dense-core vesicles are strategically localized for presynaptic modulation in the hippocampal formation and substantia nigra. Synapse *19*, 160–169. https://doi.org/10.1002/syn.890190303.
21. Paquet, L., Massie, B., and Mains, R.E. (1996). Proneuropeptide Y processing in large dense-core vesicles: manipulation of prohormone convertase expression in sympathetic neurons using adenoviruses. J. Neurosci. *16*, 964–973. https://doi.org/10.1523/jneurosci.16-03-00964.1996.
22. Stanić, D., Brumovsky, P., Fetissov, S., Shuster, S., Herzog, H., and Hökfelt, T. (2006). Characterization of neuropeptide Y2 receptor protein expression in the mouse brain. I. Distribution in cell bodies and nerve terminals. J. Comp. Neurol. *499*, 357–390. https://doi.org/10.1002/cne.21046.
23. Domingues, M.F., De Assis, D.R., Piovesan, A.R., Belo, C.A.D., and Da Costa, J.C. (2018). Peptide YY (3–36) modulates intracellular calcium through activation of the phosphatidylinositol pathway in hippocampal neurons. Neuropeptides *67*, 1–8. https://doi.org/10.1016/j.npep.2017.11.003.
24. El Bahh, B., Balosso, S., Hamilton, T., Herzog, H., Beck-Sickinger, A.G., Sperk, G., Gehlert, D.R., Vezzani, A., and Colmers, W.F. (2005). The anti-epileptic actions of neuropeptide Y in the hippocampus are mediated by Y_2 and not Y_5 receptors. Eur. J. Neurosci. *22*, 1417–1430. https://doi.org/10.1111/j.1460-9568.2005.04338.x.
25. Greber, S., Schwarzer, C., and Sperk, G. (1994). Neuropeptide Y inhibits potassium-stimulated glutamate release through Y_2 receptors in rat hippocampal slices *in vitro*. Br. J. Pharmacol. *113*, 737–740. https://doi.org/10.1111/j.1476-5381.1994.tb17055.x.
26. Melin, E., Andersson, M., Gøtzsche, C.R., Wickham, J., Huang, Y., Szczygiel, J.A., Boender, A., Christiansen, S.H., Pinborg, L., Woldbye, D.P.D., and Kokaia, M. (2023). Combinatorial gene therapy for epilepsy: Gene sequence positioning and AAV serotype influence expression and inhibitory effect on seizures. Gene Ther. *30*, 649–658.
27. RöDer, C., Schwarzer, C., Vezzani, A., Gobbi, M., Mennini, T., and Sperk, G. (1996). Autoradiographic analysis of neuropeptide Y receptor binding sites in the rat hippocampus after kainic acid-induced limbic seizures. Neuroscience *70*, 47–55. https://doi.org/10.1016/0306-4522(95)00332-d.
28. Furtinger, S., Pirker, S., Czech, T., Baumgartner, C., Ransmayr, G., and Sperk, G. (2001). Plasticity of Y1 and Y2 Receptors and Neuropeptide Y Fibers in Patients with Temporal Lobe Epilepsy. J. Neurosci. *21*, 5804–5812.
29. Kullmann, D.M., Schorge, S., Walker, M.C., and Wykes, R.C. (2014). Gene therapy in epilepsy-is it time for clinical trials? Nat. Rev. Neurol. *10*, 300–304. https://doi.org/10.1038/nrneurol.2014.43.
30. Simonato, M. (2014). Gene therapy for epilepsy. Epilepsy Behav. *38*, 125–130. https://doi.org/10.1016/j.yebeh.2013.09.013.
31. Englot, D.J. (2018). A modern epilepsy surgery treatment algorithm: Incorporating traditional and emerging technologies. Epilepsy Behav. *80*, 68–74. https://doi.org/10.1016/j.yebeh.2017.12.041.
32. Ling, Q., Herstine, J.A., Bradbury, A., and Gray, S.J. (2023). AAV-based in vivo gene therapy for neurological disorders. Nat. Rev. Drug Discov. *22*, 789–806. https://doi.org/10.1038/s41573-023-00766-7.
33. Bennett, J., Wellman, J., Marshall, K.A., McCague, S., Ashtari, M., Distefano-Pappas, J., Elci, O.U., Chung, D.C., Sun, J., Wright, J.F., et al. (2016). Safety and durability of effect of contralateral-eye administration of AAV2 gene therapy in patients with childhood-onset blindness caused by RPE65 mutations: a follow-on phase 1 trial. Lancet *388*, 661–672. https://doi.org/10.1016/s0140-6736(16)30371-3.
34. Costa Verdera, H., Kuranda, K., and Mingozzi, F. (2020). AAV Vector Immunogenicity in Humans: A Long Journey to Successful Gene Transfer. Mol. Ther. *28*, 723–746. https://doi.org/10.1016/j.ymthe.2019.12.010.
35. Woldbye, D.P.D., Angehagen, M., Gøtzsche, C.R., Elbrønd-Bek, H., Sørensen, A.T., Christiansen, S.H., Olesen, M.V., Nikitidou, L., Hansen, T.V.O., Kanter-Schlifke, I., and Kokaia, M. (2010). Adeno-associated viral vector-induced overexpression of neuropeptide Y Y2 receptors in the hippocampus suppresses seizures. Brain *133*, 2778–2788. https://doi.org/10.1093/brain/awq219.

36. Melin, E., Nanobashvili, A., Avdic, U., Gøtzsche, C.R., Andersson, M., Woldbye, D. P.D., and Kokaia, M. (2019). Disease Modification by Combinatorial Single Vector Gene Therapy: A Preclinical Translational Study in Epilepsy. Mol. Ther. Methods Clin. Dev. *15*, 179–193. https://doi.org/10.1016/j.omtm.2019.09.004.

37. Richichi, C., Lin, E.-J.D., Stefanin, D., Colella, D., Ravizza, T., Grignaschi, G., Veglianese, P., Sperk, G., During, M.J., and Vezzani, A. (2004). Anticonvulsant and Antiepileptogenic Effects Mediated by Adeno-Associated Virus Vector Neuropeptide Y Expression in the Rat Hippocampus. J. Neurosci. *24*, 3051–3059. https://doi.org/10.1523/jneurosci.4056-03.2004.

38. Gariboldi, M., Conti, M., Cavaleri, D., Samanin, R., and Vezzani, A. (1998). Anticonvulsant properties of BIBP3226, a non-peptide selective antagonist at neuropeptide Y Y_1 receptors. Eur. J. Neurosci. *10*, 757–759. https://doi.org/10.1046/j.1460-9568.1998.00061.x.

39. Benmaamar, R., Pham-Lê, B., Marescaux, C., Pedrazzini, T., and Depaulis, A. (2003). Induced down-regulation of neuropeptide Y-Y1 receptors delays initiation of kindling. Eur. J. Neurosci. *18*, 768–774. https://doi.org/10.1046/j.1460-9568.2003.02810.x.

40. Lin, E.J.D., Young, D., Baer, K., Herzog, H., and During, M.J. (2006). Differential Actions of NPY on Seizure Modulation via Y1 and Y2 Receptors: Evidence from Receptor Knockout Mice. Epilepsia *47*, 773–780. https://doi.org/10.1111/j.1528-1167.2006.00500.x.

41. George, L.A., Sullivan, S.K., Giermasz, A., Rasko, J.E.J., Samelson-Jones, B.J., Ducore, J., Cuker, A., Sullivan, L.M., Majumdar, S., Teitel, J., et al. (2017). Hemophilia B Gene Therapy with a High-Specific-Activity Factor IX Variant. N. Engl. J. Med. *377*, 2215–2227. https://doi.org/10.1056/nejmoa1708538.

42. Tian, L., Hires, S.A., and Looger, L.L. (2012). Imaging Neuronal Activity with Genetically Encoded Calcium Indicators. Cold Spring Harbor Protoc. *2012*, 647–656. https://doi.org/10.1101/pdb.top069609.

43. Grienberger, C., and Konnerth, A. (2012). Imaging Calcium in Neurons. Neuron *73*, 862–885. https://doi.org/10.1016/j.neuron.2012.02.011.

44. Colombi, I., Mahajani, S., Frega, M., Gasparini, L., and Chiappalone, M. (2013). Effects of antiepileptic drugs on hippocampal neurons coupled to micro-electrode arrays. Front. Neuroeng. *6*, 10. https://doi.org/10.3389/fneng.2013.00010.

45. Obien, M.E.J., Deligkaris, K., Bullmann, T., Bakkum, D.J., and Frey, U. (2014). Revealing neuronal function through microelectrode array recordings. Front. Neurosci. *8*, 423. https://doi.org/10.3389/fnins.2014.00423.

46. Doods, H., Gaida, W., Wieland, H.A., Dollinger, H., Schnorrenberg, G., Esser, F., Engel, W., Eberlein, W., and Rudolf, K. (1999). BIIE0246: A selective and high affinity neuropeptide Y Y2 receptor antagonist. Eur. J. Pharmacol. *384*, R3–R5. https://doi.org/10.1016/s0014-2999(99)00650-0.

47. Otto, J.F., Kimball, M.M., and Wilcox, K.S. (2002). Effects of the Anticonvulsant Retigabine on Cultured Cortical Neurons: Changes in Electroresponsive Properties and Synaptic Transmission. Mol. Pharmacol. *61*, 921–927. https://doi.org/10.1124/mol.61.4.921.

48. Large, C.H., Sokal, D.M., Nehlig, A., Gunthorpe, M.J., Sankar, R., Crean, C.S., Vanlandingham, K.E., and White, H.S. (2012). The spectrum of anticonvulsant efficacy of retigabine (ezogabine) in animal models: Implications for clinical use. Epilepsia *53*, 425–436. https://doi.org/10.1111/j.1528-1167.2011.03364.x.

49. Stanley, B.G., and Leibowitz, S.F. (1985). Neuropeptide Y injected in the paraventricular hypothalamus: a powerful stimulant of feeding behavior. Proc. Natl. Acad. Sci. USA *82*, 3940–3943. https://doi.org/10.1073/pnas.82.11.3940.

50. Luquet, S., Perez, F.A., Hnasko, T.S., and Palmiter, R.D. (2005). NPY/AgRP Neurons Are Essential for Feeding in Adult Mice but Can Be Ablated in Neonates. Science *310*, 683–685. https://doi.org/10.1126/science.1115524.

51. Zhang, L., Hernandez-Sanchez, D., and Herzog, H. (2019). Regulation of feeding related behaviours by Arcuate neuropeptide Y neurons. Endocrinology *160*, 1411–1420. https://doi.org/10.1210/en.2019-00056.

52. Lothman, E.W., Hatlelid, J.M., Zorumski, C.F., Conry, J.A., Moon, P.F., and Perlin, J. B. (1985). Kindling with rapidly recurring hippocampal seizures. Brain Res. *360*, 83–91. https://doi.org/10.1016/0006-8993(85)91223-5.

53. Lothman, E.W., and Williamson, J.M. (1993). Rapid kindling with recurrent hippocampal seizures. Epilepsy Res. *14*, 209–220. https://doi.org/10.1016/0920-1211(93)90045-9.

54. Cambiaghi, M., Cursi, M., Monzani, E., Benfenati, F., Comi, G., Minicucci, F., Valtorta, F., and Leocani, L. (2013). Temporal evolution of neurophysiological and behavioral features of synapsin I/II/III triple knock-out mice. Epilepsy Res. *103*, 153–160. https://doi.org/10.1016/j.eplepsyres.2012.07.012.

55. Love, S.A., Marie, D., Roth, M., Lacoste, R., Nazarian, B., Bertello, A., Coulon, O., Anton, J.-L., and Meguerditchian, A. (2016). The average baboon brain: MRI templates and tissue probability maps from 89 individuals. NeuroImage *132*, 526–533. https://doi.org/10.1016/j.neuroimage.2016.03.018.

56. Frahm, H.D., and Zilles, K. (1994). Volumetric comparison of hippocampal regions in 44 primate species. J. Hirnforsch. *35*, 343–354.

57. Gu, B., and Dalton, K.A. (2017). Models and detection of spontaneous recurrent seizures in laboratory rodents. Zool. Res. *38*, 171–179. https://doi.org/10.24272/j.issn.2095-8137.2017.042.

58. Campos, G., Fortuna, A., Falcão, A., and Alves, G. (2018). In vitro and in vivo experimental models employed in the discovery and development of antiepileptic drugs for pharmacoresistant epilepsy. Epilepsy Res. *146*, 63–86. https://doi.org/10.1016/j.eplepsyres.2018.07.008.

59. Sperk, G., Lassmann, H., Baran, H., Kish, S.J., Seitelberger, F., and Hornykiewicz, O. (1983). Kainic acid induced seizures: Neurochemical and histopathological changes. Neuroscience *10*, 1301–1315. https://doi.org/10.1016/0306-4522(83)90113-6.

60. Sharma, A.K., Reams, R.Y., Jordan, W.H., Miller, M.A., Thacker, H.L., and Snyder, P.W. (2007). Mesial Temporal Lobe Epilepsy: Pathogenesis, Induced Rodent Models and Lesions. Toxicol. Pathol. *35*, 984–999. https://doi.org/10.1080/01926230701748305.

61. Baudouin, S.J., Giles, A.R., Pearson, N., Deforges, S., He, C., Boileau, C., Partouche, N., Borta, A., Gautron, J., Wartel, M., et al. (2024). A novel AAV9-dual microRNA-vector targeting GRIK2 in the hippocampus as a treatment for mesial temporal lobe epilepsy. Mol. Ther. Methods Clin. Dev. *32*, 101342. https://doi.org/10.1016/j.omtm.2024.101342.

62. Boileau, C., Deforges, S., Peret, A., Scavarda, D., Bartolomei, F., Giles, A., Partouche, N., Gautron, J., Viotti, J., Janowitz, H., et al. (2023). GluK2 Is a Target for Gene Therapy in Drug-Resistant Temporal Lobe Epilepsy. Ann. Neurol. *94*, 745–761. https://doi.org/10.1002/ana.26723.

63. Royo, N.C., Vandenberghe, L.H., Ma, J.-Y., Hauspurg, A., Yu, L., Maronski, M., Johnston, J., Dichter, M.A., Wilson, J.M., and Watson, D.J. (2008). Specific AAV serotypes stably transduce primary hippocampal and cortical cultures with high efficiency and low toxicity. Brain Res. *1190*, 15–22. https://doi.org/10.1016/j.brainres.2007.11.015.

64. Tsai, D., Sawyer, D., Bradd, A., Yuste, R., and Shepard, K.L. (2017). A very large-scale microelectrode array for cellular-resolution electrophysiology. Nat. Commun. *8*, 1802. https://doi.org/10.1038/s41467-017-02009-x.

65. Klapstein, G.J., and Colmers, W.F. (1997). Neuropeptide Y Suppresses Epileptiform Activity in Rat Hippocampus In Vitro. J. Neurophysiol. *78*, 1651–1661. https://doi.org/10.1152/jn.1997.78.3.1651.

66. El Bahh, B., Cao, J.Q., Beck-Sickinger, A.G., and Colmers, W.F. (2002). Blockade of neuropeptide Y_2 receptors and suppression of NPY's anti-epileptic actions in the rat hippocampal slice by BIIE0246. Br. J. Pharmacol. *136*, 502–509. https://doi.org/10.1038/sj.bjp.0704751.

67. Cattaneo, S., Verlengia, G., Marino, P., Simonato, M., and Bettegazzi, B. (2020). NPY and Gene Therapy for Epilepsy: How, When. Front. Mol. Neurosci. *13*, 608001. https://doi.org/10.3389/fnmol.2020.608001.

68. Ledri, M., Sørensen, A.T., Erdelyi, F., Szabo, G., and Kokaia, M. (2011). Tuning afferent synapses of hippocampal interneurons by neuropeptide Y. Hippocampus *21*, 198–211. https://doi.org/10.1002/hipo.20740.

69. Liu, Y.-Q., Yu, F., Liu, W.-H., He, X.-H., and Peng, B.-W. (2014). Dysfunction of hippocampal interneurons in epilepsy. Neurosci. Bull. *30*, 985–998. https://doi.org/10.1007/s12264-014-1478-4.

70. Malmström, R.E., Lundberg, J.O.N., and Weitzberg, E. (2002). Autoinhibitory function of the sympathetic prejunctional neuropeptide Y Y2 receptor evidenced by BIIE0246. Eur. J. Pharmacol. *439*, 113–119. https://doi.org/10.1016/s0014-2999(02)01371-7.

71. Russo, A.F. (2017). Overview of Neuropeptides: Awakening the Senses? Headache *57*, 37–46. https://doi.org/10.1111/head.13084.

72. Cattaneo, S., Bettegazzi, B., Crippa, L., Asth, L., Regoni, M., Soukupova, M., Zucchini, S., Cantore, A., Codazzi, F., Valtorta, F., and Simonato, M. (2024). Gene therapy for epilepsy targeting neuropeptide Y and its Y2 receptor to dentate gyrus granule cells. EMBO Rep. *25*, 4387–4409. https://doi.org/10.1038/s44319-024-00244-0.

73. Yang, L., Scott, K.A., Hyun, J., Tamashiro, K.L., Tray, N., Moran, T.H., and Bi, S. (2009). Role of Dorsomedial Hypothalamic Neuropeptide Y in Modulating Food Intake and Energy Balance. J. Neurosci. *29*, 179–190. https://doi.org/10.1523/jneurosci.4379-08.2009.

74. Tiesjema, B., La Fleur, S.E., Luijendijk, M.C.M., and Adan, R.A.H. (2009). Sustained NPY Overexpression in the PVN Results in Obesity via Temporarily Increasing Food Intake. Obesity *17*, 1448–1450. https://doi.org/10.1038/oby.2008.670.

75. Szczygieł, J.A., Danielsen, K.I., Melin, E., Rosenkranz, S.H., Pankratova, S., Ericsson, A., Agerman, K., Kokaia, M., and Woldbye, D.P.D. (2020). Gene therapy vector encoding neuropeptide Y and its receptor Y2 for future treatment of epilepsy: preclinical data in rats. Front. Mol. Neurosci. *13*, 232.

76. Song, S., Scott-Jorgensen, M., Wang, J., Poirier, A., Crawford, J., Campbell-Thompson, M., and Flotte, T.R. (2002). Intramuscular Administration of Recombinant Adeno-Associated Virus 2 α-1 Antitrypsin (rAAV-SERPINA1) Vectors in a Nonhuman Primate Model: Safety and Immunologic Aspects. Mol. Ther. *6*, 329–335. https://doi.org/10.1006/mthe.2002.0673.

77. McTiernan, C.F., Mathier, M.A., Zhu, X., Xiao, X., Klein, E., Swan, C.H., Mehdi, H., Gibson, G., Trichel, A.M., Glorioso, J.C., et al. (2007). Myocarditis following adeno-associated viral gene expression of human soluble TNF receptor (TNFRII-Fc) in baboon hearts. Gene Ther. *14*, 1613–1622. https://doi.org/10.1038/sj.gt.3303020.

78. Chng, K., Larsen, S.R., Zhou, S., Wright, J.F., Martiniello-Wilks, R., and Rasko, J.E.J. (2007). Specific adeno-associated virus serotypes facilitate efficient gene transfer into human and non-human primate mesenchymal stromal cells. J. Gene Med. *9*, 22–32. https://doi.org/10.1002/jgm.990.

79. Tse, L.V., Klinc, K.A., Madigan, V.J., Castellanos Rivera, R.M., Wells, L.F., Havlik, L. P., Smith, J.K., Agbandje-Mckenna, M., and Asokan, A. (2017). Structure-guided evolution of antigenically distinct adeno-associated virus variants for immune evasion. Proc. Natl. Acad. Sci. USA *114*, E4812–E4821. https://doi.org/10.1073/pnas.1704766114.

80. Mahaney, M.C., Leland, M.M., Williams-Blangero, S., and Marinez, Y.N. (1993). Cross-sectional growth standards for captive baboons: II. Organ weight by body weight. J. Med. Primatol. *22*, 415–427. https://doi.org/10.1111/j.1600-0684.1993.tb00694.x.

81. Navarrete, A.F., Blezer, E.L.A., Pagnotta, M., de Viet, E.S.M., Todorov, O.S., Lindenfors, P., Laland, K.N., and Reader, S.M. (2018). Primate brain anatomy: new volumetric MRI measurements for neuroanatomical studies. Brain Behav. Evol. *91*, 109–117.

82. Wang, L., Calcedo, R., Bell, P., Lin, J., Grant, R.L., Siegel, D.L., and Wilson, J.M. (2011). Impact of Pre-Existing Immunity on Gene Transfer to Nonhuman Primate Liver with Adeno-Associated Virus 8 Vectors. Hum. Gene Ther. *22*, 1389–1401. https://doi.org/10.1089/hum.2011.031.

83. Snowball, A., Chabrol, E., Wykes, R.C., Shekh-Ahmad, T., Cornford, J.H., Lieb, A., Hughes, M.P., Massaro, G., Rahim, A.A., Hashemi, K.S., et al. (2019). Epilepsy Gene Therapy Using an Engineered Potassium Channel. J. Neurosci. *39*, 3159–3169. https://doi.org/10.1523/JNEUROSCI.1143-18.2019.

84. Agostinho, A.S., Mietzsch, M., Zangrandi, L., Kmiec, I., Mutti, A., Kraus, L., Fidzinski, P., Schneider, U.C., Holtkamp, M., Heilbronn, R., and Schwarzer, C. (2019). Dynorphin-based "release on demand" gene therapy for drug-resistant temporal lobe epilepsy. EMBO Mol. Med. *11*, e9963. https://doi.org/10.15252/emmm.201809963.

85. Blümcke, I., Beck, H., Lie, A.A., and Wiestler, O.D. (1999). Molecular neuropathology of human mesial temporal lobe epilepsy. Epilepsy Res. *36*, 205–223. https://doi.org/10.1016/s0920-1211(99)00052-2.

86. Riban, V., Bouilleret, V., Pham-Lê, B.T., Fritschy, J.M., Marescaux, C., and Depaulis, A. (2002). Evolution of hippocampal epileptic activity during the development of hippocampal sclerosis in a mouse model of temporal lobe epilepsy. Neuroscience *112*, 101–111. https://doi.org/10.1016/s0306-4522(02)00064-7.

87. Gitler, D., Takagishi, Y., Feng, J., Ren, Y., Rodriguiz, R.M., Wetsel, W.C., Greengard, P., and Augustine, G.J. (2004). Different Presynaptic Roles of Synapsins at Excitatory and Inhibitory Synapses. J. Neurosci. *24*, 11368–11380. https://doi.org/10.1523/jneurosci.3795-04.2004.